Title: Testosterone-Induced Metabolic Changes in Seminal Vesicle Epithelial cells Alter Plasma Components to Enhance Sperm Fertility

Authors: Takahiro Yamanaka[1], Zimo Xiao[1], Natsumi Tsujita[1], Mahmoud Awad[1,2], Takashi Umehara[1], Masayuki Shimada[1,3*]

Affiliations:

[1] Graduate School of Integrated Sciences for Life, Hiroshima University; Higashihiroshima, Hiroshima, Japan

[2] Department of Histology, Faculty of Veterinary Medicine, South Valley University; Qena, Egypt

[3] Graduate School of Innovation and Practice for Smart Society, Hiroshima University; Higashihiroshima, Hiroshima, Japan

*Corresponding author. Masayuki Shimada, Ph.D. E-mail: mashimad@hiroshima-u.ac.jp, Tel/Fax: (+81)-824-24-7899

One Sentence Summary: Testosterone induces ACLY expression in seminal vesicle, a key factor of forming seminal plasma to acquire *in vivo* fertilization ability of sperm.

Abstract:

Male infertility depends on both sperm and seminal plasma and is induced by aging. In this study, male infertility was examined with seminal plasma and its synthesis mechanism. The factors ensuring *in vivo* fertilization potential was secreted from seminal vesicle where the factors were synthesized in an androgen-dependent manner. Androgen increased glucose uptake and glycolytic capacity in seminal vesicles, which caused activation of oleic acid synthesis rather than mitochondrial ATP synthesis. ACLY was identified as a key player in this metabolic mechanism for producing oleic acid that was incorporated into the sperm and enhanced fertilization potential *in vivo*. In conclusion, an important role of testosterone-induced metabolic pathways in the seminal vesicle was to ensure the synthesis of oleic acid, which is essential for sperm fertilization *in vivo*. These results provide new perspectives for the development of biochemical markers of semen to assess male fertility and for artificial insemination techniques.

Main Text:

INTRODUCTION

Infertility is defined by the World Health Organization (WHO) as the failure to conceive within 12 months despite contraceptive-free sexual intercourse. Its prevalence has increased over the decades and now accounts for 17.5% of couples worldwide *(1)*. The male partner is thought to be solely or in combination responsible for 50% of infertility cases, and the male factor in the etiology of infertility is highly recognized. The male fertility depends largely on the quality of semen composed of sperm and seminal plasma and decreases with aging.

Spermatogenesis, the process by which mature sperm are generated, takes place partially in the testis, where the characteristic sperm morphology of the head, middle, and tail is formed. Within testis however, sperm are functionally immature and cannot penetrate an oocyte until they undergo a maturation process that occurs during their passage through the epididymis *(2–4)*. Sperm recovered from the epididymis can fertilize a mature oocyte *in vitro* but cannot maintain sustained liner motility required for migration from the uterus to the oviduct *(5, 6)*. Thus, when epididymal sperm are artificially inseminated to the cervix or uterus, fertilization rates are low *(7–9)*. However, when epididymal sperm are mixed with seminal plasma at the time of ejaculation or when sperm are exposed to seminal plasma *in vitro*, even for only a brief period of time, they acquire *in vivo* fertilization potential and are capable of passing through the female reproductive tract and fertilizing ovulated oocyte *in vivo (10)*. Thus, sperm formation occurs in the testis, they mature in the epididymis, but only acquire the *in vivo* fertilization ability after exposure to seminal plasma.

Seminal plasma is mainly produced in the seminal vesicles (approximately 65-75%), with approximately 20-30% produced by the prostate, and small amounts secreted by the bulbourethral and urethral glands *(11)*. Seminal plasma or TGFβ, a component of seminal plasma, increases antigen-specific Treg cells in uterus of mice and humans which induce immune tolerance, resulting in pregnancy *(12, 13)*. Furthermore, SVS2 that is secreted from the seminal vesicle is also known to be required for sperm to escape attack by the female immune system in uterus *(14)*. In addition, seminal plasma is known to contain various biochemical components that support sperm metabolism, including lipids and organic acids. Specifically, Rosecrans et al. *(15)* found significant differences in the levels of most biochemical components in seminal plasma compared

to blood, with specific factors like fructose being rarely detected in blood but abundant in seminal plasma. Our previous studies *(16–18)* documented that seminal plasma also contains creatine, and fatty acids, that are taken up by sperm within minutes. These substances play crucial roles in regulating sperm metabolic pathways and enhancing sperm motility. Collectively these observations indicate that seminal plasma not only alters the female immune system to protect sperm but also directly influences sperm metabolic pathways, facilitating the transformation of sperm capable of *in vivo* fertilization.

Some specific factors that male accessory glands contribute to seminal plasma and impact male fertility have been elucidated. For example, surgical removal of seminal vesicles in male mice and rats was associated with infertility *(14, 19, 20)*. The observation that fructose *(21)* and citric acid *(22)* concentrations in seminal plasma of control mice and rats are higher than in castrated animals indicates that specific functions of the accessory glands might be affected by testicular-derived testosterone that is known to activate the intracellular androgen receptor (AR;NR3C4), required for gene regulation of transcription. AR-deficient mice have been found to be infertile *(23)*, and long-term administration of androgen receptor antagonists, like flutamide, abolished male fertility *(24, 25)*. AR-deficient mice and transcriptome analyses have identified specific targets of AR *(26, 27)*. In both mice and human, androgen levels decrease with aging, and their concentrations have been reported to cause a decrease in male fertility, especially ejaculated sperm motility. Therefore, the reduction of androgen concentrations may affect the metabolic mechanisms of the accessory reproductive organs and alter the composition of seminal plasma with aging. However, the metabolic mechanisms that impact sperm functions are governed by a complex of enzymatic reactions and therefore, the intricate interplay between testosterone and seminal plasma synthesis in the accessory reproductive organs requires further investigation.

In this study, we first performed various bioassays to identify which accessory glands are essential for sperm fertility. Subsequently, comparative *in vivo* and *in vitro* analyses were performed using a hypoandrogenic model. In addition, biochemical and molecular techniques such as RNA-seq, flux analysis, mass spectrometry, and knockdown experiments were employed. These analyses reveal the pathways by which seminal vesicles synthesize seminal plasma, ensure fertilization ability, and provide new therapeutic and preventive strategies for male infertility.

Seminal vesicle and prostate-derived fluids induce functional sperm motility

A bioassay using epididymal sperm that had not been exposed to seminal plasma was done to clarify the effect of seminal plasma on sperm functions. For this bioassay, fluids were prepared from seminal vesicle secretion and homogenized prostate tissues, and then the fluid was mixed with the basic medium, Human Tubal Fluid (HTF) medium in various proportions (Fig.1A-D). The addition of seminal vesicle secretion alone to the basic medium (HTF medium) significantly increased the rate of sperm linear motility (LIN) compared to the HTF medium alone (Fig.1D). The straight line velocity (VSL) of those sperm was also significantly increased (Fig.1C). This significant increase in straightening of sperm by the seminal vesicle-derived secretion was further significantly positively affected by the addition of prostate extract 1:9 or 2:8 to the seminal vesicle secretion (Fig.1C,D). However, no significant improvement in straightness was observed with the mixture of prostate extract alone (Fig.1C,D). These results clearly indicate that sperm exposure to seminal plasma factors significantly improves sperm linear motility and that this positive effect is mainly due to the seminal vesicle secretory factors.

The functions of male accessory reproductive organs are regulated by androgens. Therefore, to elucidate whether the seminal vesicle factors, which enhance sperm linear motility, are synthesized in an androgen-dependent manner, bioassays were performed using seminal vesicle secretions collected from control mice or mice treated for 7 consecutive days with flutamide, an androgen receptor antagonist, and sperm collected from the epididymis of mice not treated with flutamide (Fig.1E). The results showed that LIN and VSL were significantly reduced in the seminal vesicle secretions from flutamide-treated mice (Flutamide) compared to the control mice (Ctrl) (Fig.1F,G). The reduction of sperm linier motility speed (VSL) was also significantly lower in the sperm treated with seminal vesicle secretions from over 12 months old mice that showed low circular testosterone level as compared with the sperm treated with seminal vesicle secretions from young adult mice (3 months old mice) (Supplemental Fig.1A,B). Furthermore, JC-1 staining to measure mitochondrial membrane potential, which is important for sperm linear motility, showed significantly lower mitochondrial membrane potential activity in sperm treated with the secretions of seminal vesicles from flutamide-treated mice (Fig.1H). These results indicated that androgen-dependent changes in seminal vesicle functions alter the levels/activity of seminal vesicle secretion factors, which regulate sperm linear motility. The changes of seminal vesicle

functions were also induced with aging.

Testosterone-androgen receptor activity suppresses the proliferation of seminal vesicle epithelial cells

To understand the difference between seminal vesicles that secrete factors for enhancing sperm linear motility and those that are impaired in this function, we performed histological analysis of seminal vesicles recovered from mice treated and non-treated with flutamide. In control mice, the seminal vesicle epithelial cells were in a single layer, and androgen receptors were localized in the nuclei of seminal vesicle epithelial cells (Fig.2A). However, in mice treated with continuous administration of flutamide, seminal vesicle epithelial cells were multilayered, and the strong accumulation of androgen receptors in nucleus was not observed (Fig.2A). To investigate the cause of this multilayering of cells, we performed Ki67 staining, a marker of cell proliferation, and apoptosis detection by TUNEL staining (Fig.2B). The results showed that the percentage of Ki67-positive cells increased significantly after treatment with flutamide, but the percentage of TUNEL-positive cells did not change, suggesting that the testosterone-androgen receptor pathway is responsible for the inhibition of proliferation of seminal vesicle epithelial cells (Fig.2C). These changes of abnormal morphology and high proliferation activity were also observed in seminal vesicle of more than 12 months old mice that showed the low level of testosterone in serum (Supplemental Figure 1C-E). Therefore, seminal vesicle epithelial cells were collected and cultured in primary culture as shown in Fig. 2D, and the changes in cell number were counted and cell cycle was analyzed by flow cytometry. When cultured without testosterone (c), the number of seminal vesicle epithelial cells increased in a day-dependent manner. However, the addition of testosterone significantly decreased the number of seminal vesicle epithelial cells during the 8-day culture period in a concentration-dependent manner (Fig.2E). Flow cytometric analysis of the cell cycle on day 7 showed that the G0/G1 phase was significantly increased and the G2/M1 phase was significantly decreased by the addition of testosterone (Fig. 2F,G). These results indicate that seminal vesicle epithelial cells are inhibited in cell division by the testosterone-androgen receptor pathway.

Testosterone alters metabolic gene expression in seminal vesicle epithelial cells

To better understand the roles of testosterone in suppressing proliferation of seminal vesicle epithelial cells, RNA sequencing was done using the epithelial cells cultured with or without testosterone. DEG (Differential Expressed Genes) analysis revealed that a total of 23,459 genes were identified, including 997 upregulated genes and 3463 downregulated genes in seminal vesicle epithelial cells by testosterone relative to control (Fig.3A). Genes largely upregulated by testosterone included those already reported in seminal vesicles *(14, 19, 28)*, such as the Seminal Vesicle Secretion (*Svs*) family (*Svs1~6*), *Pate4*, *Spinkl*, *Ceacam10*, and *Sva* (Fig.3B,C). Therefore, the primary culture of seminal vesicle epithelial cells used in this experiment was considered to maintain the characteristics of seminal vesicle epithelial cells *in vivo*. Many genes were downregulated by testosterone, and those with a high rate of variation included collagen synthase and *Mmp2*, which are involved in extracellular matrix formation (Fig.3C). However, KEGG analysis, rather than individual genes, was used to predict functions altered by testosterone, and it was found that the expression of genes involved in the metabolic pathway was the most highly affected by testosterone (Fig.3D). Because there is a close relationship between cell proliferation and metabolic activity, and between metabolic substrates in seminal plasma and sperm motility, we hypothesized that testosterone induced changes in seminal vesicle epithelial cell metabolism alter the components of seminal plasma to mediate the enhancement of sperm motility.

Testosterone sifts metabolic activity of seminal vesicle epithelial cells

In the presence of testosterone, the addition of glucose significantly activated glycolysis as compared with that in epithelial cells cultured without testosterone (Fig.4A,B). However, there was no difference in the glycolytic capacity, indicating that testosterone may increase glucose metabolism but does not to enhance the expression of a group of enzymes involved in the glycolytic pathway. To determine the metabolic fate of glycolytic end products, seminal vesicle epithelial cells were cultured with and without testosterone and then concentrations of pyruvate and lactate were measured. The concentration of pyruvate was significantly decreased by the addition of testosterone; however, the concentration of lactate was not significantly changed (Fig.4D,E). Therefore, we analyzed mitochondrial metabolism using a flux analyzer, predicting that

more glucose is metabolized, pyruvate is synthesized in response to testosterone, and is further metabolized in the mitochondria. However, measuring mitochondrial respiratory metabolism with a Flux analyzer, the basal respiratory rate (the activity of the electron transport chain) was significantly decreased by testosterone (Fig.4F-I). ATP production was also significantly suppressed exposure to testosterone. Furthermore, the maximum respiration and spare respiration capacity were also significantly decreased in response to testosterone treatment, suggesting that testosterone does not educe transient enzyme activity in mitochondria, but to rather weakens the metabolic pathway of the mitochondrial TCA cycle and/or the electron transport chain due to the changes in gene expression patterns in seminal vesicle epithelial cells.

Testosterone causes changes in the expression of genes encoding enzymes involved in glucose catabolism and anabolism

The expression of genes involved in glucose catabolism and anabolism in the *in vitro* culture system of seminal vesicle epithelial cells was analyzed by qPCR (Fig.5). The gene expression of glucose transporter (*Glut*) and enzymes involved in the glycolytic pathway were not significantly affected by testosterone, consistent with the results of metabolic flux analysis, which showed that the glycolytic pathway was not enhanced despite the activation of the glycolysis. Furthermore, the expression of genes encoding enzymes involved in the TCA cycle in mitochondria was also not significantly affected by testosterone, but the expression of enzymes involved in the electron transport chain was significantly decreased. Interestingly, the expression of *Acly*, that encodes an enzyme that reconverts citric acid formed in the TCA cycle to Acetyl CoA and induces cholesterol synthesis and fatty acid synthesis, was significantly increased by testosterone. Although *Hmgcr*, which encodes the rate-limiting enzyme involved in cholesterol synthesis, was unchanged, the expression of *Acc*, which encodes the rate-limiting enzyme for fatty acid synthesis, was significantly upregulated by testosterone. These characteristic testosterone-induced changes in gene expression observed in cultured cells were also detected by ACLY immunostaining of *in vivo* seminal vesicle samples (Supplemental Figure 2). Specifically, the expression of genes encoding a group of enzymes of the electron transport chain was significantly upregulated by continuous flutamide administration *in vivo*, whereas the gene expression of *Acly* and *Acc* was significantly decreased by flutamide administration. Immunostaining results showed that ACLY

was detected specifically in seminal vesicle epithelial cells, and their staining appeared to be reduced by flutamide treatment. The lower level of ACLY was also observed in seminal vesicle epithelial cells of over 12 months old mice (Supplemental Figure 2B).

Mechanism of testosterone-induced enhancement of glucose uptake and thereby fatty acid synthesis

The effect of testosterone on glucose uptake in seminal vesicle epithelial cells was analyzed using fluorescence-labeled glucose. As expected from the results of flux metabolic analyses, testosterone treatment significantly increased glucose uptake (Supplemental Figure 3A). Because the expression of each *Glut* family gene encoding glucose transporters was not altered by testosterone (Fig.5), we focused on GLUT4, whose cellular localization is regulated, and analyzed the effects of Indinavir, a functional inhibitor of GLUT4 *(29, 30)*. Indinavir significantly suppressed glucose uptake and significantly decreased fatty acid synthesis (the amount of fatty acids accumulated in the cell), which was increased by testosterone (Supplemental Figure 3A,B). Furthermore, immunostaining analysis of the localization of GLUT4 in seminal vesicles revealed that GLUT4 was localized outside the nucleus of seminal vesicle epithelial cells (Supplemental Figure 4), suggesting that GLUT4 was partially localized at the plasma membrane and contributed to glucose uptake, whereas in seminal vesicles from mice treated with flutamide continuously, no strong signal was detected at the presumed location of GLUT4 near the plasma membrane of seminal vesicle epithelial cells (Supplemental Figure 4). The same characteristics were observed in aged mice.

Qualitative and quantitative analysis of the fatty acids synthesis was performed by GC-MS. In seminal vesicles, C16:0, C18:0 and C18:1 were detected, in which C18:1 was decreased to an undetectible level in seminal vesicles of mice treated with the flutamide (Supplemental Figure 5A). In the cultured seminal vesicle epithelial cells, C18:1, oleic acid, was significantly increased by the addition of testosterone as observed in seminal vesicle (Supplemental Figure 3C). The expression of *Elovl6* encoding ELOVL6, which desaturates C18:0 saturated fatty acids to C18:1, was significantly up-regulated by testosterone (Supplemental Figure 3D). The testosterone-induced change was also detected in *in vivo* samples (seminal vesicle), where the expression of *Evovl6* was decreased by the flutamide treatment (Supplemental Figure 5B).

Oleic acid (18:1) is taken up by sperm and promotes their linear movement

We observed that seminal vesicles secrete testosterone-dependent factors that induce sperm to move straight and that seminal vesicle epithelial cells synthesize and secrete oleic acid in a testosterone-dependent manner. In order to examine whether oleic acid is a factor that induces sperm linear motility, we examined whether or not oleic acid is taken up by sperm and then changes of sperm motility pattern. When epididymal sperm was incubated with fluorescently labeled oleic acid, the fluorescent signal was selectively detected in the midpiece of the sperm after quenching of extracellular fluorescence (Fig.6A). The fluorescence intensity of sperm detected by flow cytometry significantly increased in a dose-dependent manner (Fig.6B, C). In oleic acid-treated sperm, VSL was significantly increased in a dose-dependent manner in the range of 0 to 50 nM (Fig.6D). LIN values were highest when 10 nM oleic acid was added (Fig.6E). To quantify metabolic changes in mitochondrial activity, a flux analyzer was used to monitor real-time changes in mitochondrial β-oxidation. A significant increase in OCR was induced by the injection of 10 nM oleic acid. Etomoxir, a β-oxidation inhibitor, significantly decreased the OCR that was induced by oleic acid (Fig.6F, Supplemental Figure 6). In situ ATP detection by BioTracker ATP-Red revealed that the percentage of sperm with high ATP production was significantly increased under the presence of oleic acid (Fig.6G).

To examine whether the addition of oleic acid to low quality of seminal plasma (collected from flutamide-treated mice) restores *in vivo* the fertilization potential of epididymal sperm, sperm treated with seminal plasma collected from control or flutamide-treated mice was used for artificial insemination. The *in vivo* fertilization rate was about 70% when sperm was treated with the seminal vesicle secretions from control mice (SV); however, the fertilization rate was significantly lower in the group that sperm was treated with the seminal vesicle secretions from flutamide-treated mice (Flu) (SV: 65.5 ± 3.8%, Flu: 39.4 ± 7.8%). Although not significant, adding oleic acid to the seminal secretions of flutamide-treated mice (Flu+OA) increased the fertilization rate to 53.1 ± 1.3% (Fig.6H).

ACLY expression is upregulated by testosterone and is essential for the metabolic shift of seminal vesicle epithelial cells that mediates sperm linear motility

ACLY is up-regulated in seminal epithelial cells as a factor that enables the utilization of citric acid from the TCA cycle for fatty acid synthesis outside the mitochondria. Therefore, we performed siRNA knockdown experiments of ACLY to clarify the impact of ACLY on the cellular metabolic shift. The addition of testosterone significantly increased the amount of ACLY protein in seminal epithelial cells (Fig.7A,B). Viral infection with siRNAs encoding *Acly*-targeted siRNAs markedly decreased the amount of ACLY (Fig.7C). This knockdown of ACLY not only increased the oxygen consumption of seminal epithelial cells in the control and testosterone-treated group, but also significantly increased the ATP production related oxygen consumption (Fig.7D,E,F). Thus, ACLY expression is associated with mitochondrial metabolic pathway activity in seminal epithelial cells. Furthermore, the knockdown of ACLY also significantly suppressed testosterone-induced fatty acid synthesis in seminal epithelial cells (Fig.7G). Supernatants from epithelial cells of the testosterone-added group induced sperm to move linearly (Fig.7H). However, the knockdown of ACLY significantly reduced the effects of the culture supernatant on sperm linear motility (Fig.7H).

This characteristic metabolic mechanism induced by testosterone is also observed in human seminal epithelial cells

To determine whether these findings in mice could be applied to humans, the commercially available human seminal vesicle epithelial cells were used for following studies (Fig.8A). The growth curves showed that cell proliferation was inhibited by 100 ng/mL of testosterone compared to the control; a pattern similar to that observed in murine seminal vesicle epithelial cells (Fig.8B). The characteristics of metabolic activity of human seminal epithelial cells were also similar to those of mice, with testosterone significantly enhancing the glycolytic pathway (Fig.8C), but significantly reducing the capacity for oxygen consumption in mitochondria (Fig.8D). Moreover, fluorescent-glucose uptake was increased by testosterone and decreased by the inhibitor of GLUT4 function (Fig.8E). Additionally, while testosterone also significantly increased fatty acid synthesis, this increase was completely abolished by the GLUT4 inhibitor (Fig.8F).

DISCUSSION

Seminal plasma has a variety of functions, including sperm transport, nutritional support, interactions with the female reproductive tract, and especially the regulation of its relationship with the female immune system. Mammalian seminal plasma is secreted mainly from the seminal vesicle and is known to be rich in cytokines, prostaglandins, and SVS family members *(31)*. For this reason, recent studies have focused on the immunomodulatory function of seminal plasma in the female reproductive tract. On the other hand, fructose and lipids in seminal plasma are the major energy sources for sperm *(32)*. However, although metabolomic analyses of seminal plasma have shown that there are metabolic substrates present at higher concentrations in seminal plasma than in blood *(15, 21, 22)*, how these substrates are synthesized and specifically how they alter sperm motility has not been determined. Moreover, though the motility of ejaculated spermatozoa is known to decrease with aging, few reports have revealed age-related changes in the seminal vesicle glands, which are responsible for seminal plasma synthesis.

In this study, we focused on the reproductive organs that synthesize seminal vesicle secretion as target organs for testosterone, and found that factors formed by testosterone-dependent metabolic changes in seminal vesicles activate sperm mitochondria and enhance their linear motility. Testosterone is known to activate intracellular ARs and alter intracellular metabolic pathways in skeletal muscle *(33)*, prostate cells *(34)* and cardiomyocytes *(30)*. ARs are known to directly regulate the expression of glycolytic and lipid metabolic genes *(30, 35, 36)*. In the present study, the nuclear localization of AR in seminal vesicle epithelial cells (i.e., functioning as a transcription factor) and the activation of the glycolytic system by testosterone were similar to those in the above cell types. Interestingly, however, in the seminal vesicle epithelial cells, expression of *Glut* family members was unchanged but GLUT4 localization was altered in a testosterone-dependent manner to promote glucose uptake. Such gene expression-independent effects of testosterone on glucose metabolism have also been reported in skeletal muscle, liver, and adipose tissue, where testosterone leads to the phosphorylation of GLUT4 and enhances its translocation to the plasma membrane *(37, 38)*. This is consistent with the results of our metabolic flux analyses, that show testosterone increases the rate of glycolysis in seminal vesicle epithelial cells by increasing glucose uptake rather than by increasing glycolytic capacity. We

further confirmed that GLUT4 is the transporter that mediates this glucose uptake using indinavir, a GLUT4-specific inhibitor.

In seminal epithelial cells, ATP production was low and cell proliferation was suppressed despite testosterone-induced activation of the glycolytic system. We hypothesized that this could be explained by the testosterone-dependent regulation of genes involved in mitochondrial metabolism, including the up-regulation of ACLY, a strategic enzyme that links the glycolytic system with lipid metabolism. Manipulation of ACLY expression in mouse myoblasts and embryonic stem cells has been shown to alter the TCA cycle into a "non-normal cycle" *(39)*. One advantage of the non-normal TCA cycle is its ability to retain carbon instead of burning it and to regenerate the cytosolic NAD+ needed to maintain glycolysis *(39, 40)*. This suggests that ACLY activated by testosterone may inhibit proliferation of seminal epithelial cells by skipping some steps of the mitochondrial TCA cycle and minimizing ATP production.

Testosterone has been reported to cause hypertrophy of cardiac myocytes *(41, 42)*. Cell hypertrophy is partly due to the accumulation of fatty acids in the cytoplasm, which causes significant damage to cellular functions *(43, 44)*. On the other hand, the normal cell hypertrophy, especially in myofibers, involves the activation of signaling molecules such as Myc, hypoxia-inducible factor, and Pi3k-Akt-mTor, which regulate metabolic reprogramming in cancer by increasing glucose uptake in the presence of oxygen *(45–47)*. In the present study, induction of ACLY expression by testosterone not only decreased cycling in the TCA cycle, but also promoted glucose assimilation, which played an important role in fatty acid synthesis. Thus, in tissues where fatty acid synthesis is promoted, either β-oxidation-dependent ATP production in mitochondria or the secretion of fatty acids occurs to maintain cellular function *(48–50)*; providing evidence to explain why the presence of fatty acids in the cell has no adverse effect. In accessory reproductive glands, such as the prostate and seminal vesicles, the glycolytic system is activated in a testosterone-dependent, but ATP production is not enhanced and cell proliferation is not induced and the metabolites are used as a substrate for sperm motility. This may be because in the prostate, pyruvate synthesized by the glycolytic system in response to testosterone is converted to acetyl CoA, which is then converted to citric acid in the TCA cycle, citric acid is released as the main component of seminal plasma *(34)*.

The testosterone-dependent growth of cancerous prostate epithelial cells may be due to genetic mutations, such as elevated expression of the gene encoding aconitase, which converts citric acid to isocitrate, which blocks the TCA cycle and inhibits citric acid secretion *(51)*. On the other hand, in the analysis of seminal epithelial cells, testosterone treatment induced the expression of *Acc*, which encodes the rate-limiting enzyme for fatty acid synthesis, and *Elovl6*, which desaturates to oleic acid, significantly increasing total saturated fatty acid and oleic acid content. Therefore, testosterone promotes glucose conversion into fatty acids, especially oleic acid, in seminal epithelial cells. Although there is a commonality in the activation of the glycolytic system testosterone target tissues, the different expression patterns of genes involved in metabolism in mitochondria may exert their specific functions in each tissue. In addition to genes involved in fatty acid synthesis such as *Fasn* and *Elovl6*, *Acly* is also encoded in a region in close proximity in human chromosome 17 and mouse chromosome 11, suggesting that in seminal vesicle epithelial cells, this region is targeted to promote gene expression. The co-regulation of these genes in seminal vesicle epithelial cells leads to the synthesis of seminal plasma components that ensure sperm motility.

Decreased testosterone synthesis in the testes is a phenomenon observed with aging, and associated with decreased spermatogenesis*(52)*. However, the probability of obtaining sperm without ICSI or IVF is extremely low, despite the presence of sufficient numbers of sperm with normal-morphology *(53–55)*. This indicates that testosterone plays a major role not only in spermatogenesis but also in functional maturation of sperm. In this study, metabolic abnormalities induced by inhibition of androgen receptor function caused abnormal proliferation of seminal vesicle epithelial cells in aged mice. In other words, the findings of the seminal vesicle epithelial cell culture experiments and flutamide treatment may mimic the changes that occur with aging. Oleic acid synthesis by testosterone-dependent metabolic pathways was regulated in seminal vesicle epithelial cells and the oleic acid stimulated sperm motility and enhanced *in vivo* fertilization success. Thus, results of these studies document that the quality and presence of key metabolic products in seminal plasma influence male fertility. Specifically, the results open the possibility of translational studies to understand human male infertility, especially in cases of failure to conceive by natural mating or artificial insemination. Because seminal plasma contains components specific to certain male reproductive organs, differences in

protein composition may reflect pathological processes in specific organs *(56)*. However, although proteomic and metabolomic analyses of seminal plasma have been performed *(28, 56)*, the functional changes in seminal plasma, especially the effects on *in vivo* fertilization potential, have not been well understood. Differences in fatty acid concentrations, including oleic acid, in seminal plasma may provide a predictive marker for the fertilization potential of human and domestic animal semen. Furthermore, the addition of oleic acid to low-quality semen improved fertilization rates associated with artificial insemination, providing a strategy for improving artificial insemination. In our previous study, adding fatty acids to the thawing medium of frozen bull sperm improved their linear motility and viability *(18)*. The similarities between mouse and human seminal vesicle epithelial cells demonstrated in this study have strong potential for clinical application of these observations.

Overall, the results of the studies described herein strongly support the hypothesis that testosterone-dependent glucose to oleic acid conversion processes are required for normal seminal plasma functions in the seminal vesicle and normal reproductive performance in males. This study advances our understanding of the role of testosterone in glucose metabolism and fatty acid synthesis and lays the groundwork for future research and potential therapeutic interventions in reproductive biology and fertility.

MATERIALS AND METHODS

Study design

The objective of this study was to elucidate the mechanisms of sperm plasma synthesis that enhance sperm fertility. Testosterone-dependent changes in the seminal plasma function were examined by comparative analysis of adult mice and flutamide-treated mice. The bioassays of extracts from male accessory glands by epididymal sperm motility analysis were used to examine the seminal plasma components important for sperm fertilization. We also isolated the mouse seminal vesicle epithelial cultured cells, and investigated the synthesis mechanism of the seminal plasma components using RNA-seq, FluxAnalyzer, and shRNA knockdown. Finally, we performed validation using the human epithelial cells.

Chemicals and Animals

Unless otherwise noted, chemicals used in this study were purchased from Sigma-Aldrich (St. Louis, MO, USA) or Nacalai tesque (Osaka, Japan). Pregnant mare serum gonadotropin (PMSG) and human chorionic gonadotropin (hCG) were purchased from Asuka Seiyaku (Tokyo, Japan). All procedures during animal experiments were reviewed and approved by the Animal Care and Use Committee of Hiroshima University (Hiroshima, Japan; C21-9-3) and conducted according to regulations. Specific pathogen-free C57BL/6NCrl male mice or Crl: CD1 (ICR) female mice were purchased from Jackson Laboratory Japan (Kanagawa, Japan) and housed in an environmentally controlled room with a 12-hour light/dark cycle, a temperature of 23 ± 3°C, and free access to laboratory food (MF; Oriental Yeast Co., Ltd., Tokyo, Japan) and tap water. 8- to 16-week-old male or female mice were used for the experiments. Flutamide-treated mice were injected subcutaneously for 7 days with 50 µg/g (body weight) of flutamide dissolved in corn oil. Vehicle-treated mice received 100 µL of corn oil subcutaneously for 7 days. The aged males were 12 to 16 months old.

Bioassay using pseudo-seminal plasma and epididymal sperm

Prostate (mixed anterior, dorsal, lateral, and ventral) and seminal vesicles were collected from adult C57BL/6NCrl mice. Seminal vesicle secretions were obtained by pressing the seminal vesicles immediately after euthanasia. Prostatic extracts were obtained by homogenizing the prostate immediately after euthanasia. Seminal vesicle secretions and prostate extracts collected from one male mouse were dissolved in 500 µL and 200 µL of mHTF medium without BSA *(57)*, respectively, then centrifuged at 2000 × g for 5 min at room temperature, and the supernatant was collected, and protein levels were determined. The seminal vesicle secretions from flutamide-treated mice were also collected similarly.

Cauda epididymis sperm recovered from male mouse were dispersed in 500 µL of mHTF without BSA drops and centrifuged at 300 × g, 3 min to wash out epididymis-derived factors. The epididymis sperm was mixed with seminal vesicle secretion and/or prostate extract as shown in Fig.1A. In flutamide administration experiments, the final protein concentration of seminal vesicle secretion was adjusted to 10 mg/mL. The samples were incubated at 37°C for 60 min in a humidified atmosphere of 5% CO2 in air. Sperm motility patterns were then examined using

computer-assisted sperm analysis (CASA; HT CASA-Ceros II, Hamilton Thorne, Beverly, MA, USA).

Serum testosterone levels

The serum was separated from the clot by centrifugation at 1,500 × g for 15 min. Testosterone levels in the serum samples were determined by a rodent testosterone ELISA test kit (ERKR7016, Endocrine Technologies, Inc., Newark, CA, USA) according to the manufacturer's manual.

Mitochondrial activity

Mitochondrial activity of sperm was measured using a MitoPT® JC-1 Assay Kit (911, Immuno Chemistry Technologies, LLC, Bloomington, MN, USA) according to our previous study *(17)*. Briefly, sperm were incubated with 200 μL of working solution containing 5,5',6,6'-tetrachloro-1,1',3,3'-tetraethylbenzimidazolyl carbocyanine iodide (JC-1) dye at 37 °C for 30 min in the dark. The sperm suspension was centrifuged and washed twice with the base medium. After washing, the sperm pellet was resuspended in the base medium and analyzed with an Attune® NxT Acoustic Focusing Cytometer (Thermo Fisher Scientific Inc., Waltham, MA, USA) using a 488 nm laser and a filter with a bandwidth of 574/26 nm. The intensity of the average value was analyzed as the mean fluorescence intensity (MFI) of JC-1 orange aggregates. A total of 100,000 sperm events were analyzed. The sperm population is shown in Supplementary Figure 8.

Immunohistochemistry and immunofluorescence

Seminal vesicles were fixed overnight in 4% (w/v) paraformaldehyde/PBS, dehydrated in 70% (v/v) ethanol, and embedded in paraffin. Paraffin-embedded fixed sections (4 μm) were deparaffinized and hydrated with xylene and ethanol, respectively. Some slides were stained with hematoxylin and eosin (HE). For antigen retrieval, sections were placed in citrate buffer (pH 6.0), microwaved until boiling and allowed to stand at the temperature of pre-boil (95°C) for 15 minutes. Sections were incubated with 3% (v/v) hydrogen peroxide in methanol to block endogenous peroxidase and then incubated with Normal Goat Serum Blocking Solution for rabbit antibody (S-1000, Vector Laboratories, Newark, CA, USA) to block nonspecific sites. The

sections were then incubated overnight with primary rabbit antibodies: anti-AR antibody (1:100; ab133273; Abcam, Cambridge, UK), anti-Ki67 antibody (1:1000; ab15580; Abcam) or anti-ACLY antibody (1:200; ab40793; Abcam). Positive signals were visualized by DAB (3,3′-Diaminobenzidine, 040-27001, Fujifilm Wako, Osaka, Japan) using the VECTASTAINE LifeABC kit (PK-6101, Vector Laboratories) according to the manufacturer's protocol. Apoptotic cells (including fragmented DNA) were detected using the In Situ Cell Death Detection Kit POD (11684817910, Roche Ltd., Basel, Switzerland) according to manufacturer's protocol. Nuclei were visualized with hematoxylin (Sakura Finetek, Tokyo, Japan). Ki-67 and apoptotic positive cells were quantified using ImageJ software.

For immunofluorescence, after blocking nonspecific sites, the sections were incubated with a primary antibody: anti-GLUT4 antibody (1:200; ab33780; Abcam). After washing with 0.3% (v/v) Triton X-100 in PBS (-), Cy3-labeled goat anti-rabbit IgG (1:200, C-2306, Sigma) and DAPI (VECTESHIELD Mounting Medium with DAPI, H-1200, Vector Laboratories) were used to visualize the antigen and nuclei. Digital images were taken using an APX100 Digital Imaging System (EVIDENT, Tokyo, Japan).

Isolation and culture of seminal vesicle epithelial cells

Seminal vesicles were removed from euthanized mice, cut open vertically to expose the seminal vesicle cavity, and incubated with Hanks' balanced salt solution (HBSS; $CaCl_2 \cdot 2H_2O$ 0.185 g/L, $MgSO_4$ 0.098 g/L, KCl 0.400 g/L, KH_2PO_4 0.060 g/L, NaHCO3 0.350 g/L, NaCl 8.000 g/L, Na_2HPO_4 0.048 g/L, D-Glucose 1.0 g/L, dissolved in ultrapure water). Tissues were digested with 10 mL of HBSS containing 25 mg/mL pancreatin and 0.25% (v/v) trypsin EDTA for 1 hour at 4°C, 45 minutes at room temperature, and 15 minutes at 37°C, and epithelial cells were obtained. These were passed through a 70 µm nylon filter (352350, Corning Inc., Corning, NY, USA) and seeded into collagen-coated 12-well plates (4815-010, IWAKI, Shizuoka, Japan). Cells were cultured in DMEM/F-12, 10% fetal bovine serum (FBS; 10438-018, Thermo Fisher Scientific Inc.), 100 U/mL penicillin, 100 µg/mL streptomycin. The culture condition was 37°C, 5% CO_2, 95% air, and humidity.

Human seminal vesicle epithelial cells (4460, ScienCell Research Laboratories, Carlsbad, CA, USA) were purchased, seeded in 2 $\mu g/cm^2$ poly-L-lysine-coated plates according to

manufacturer's protocol, and cultured in epithelial cell medium (4101, ScienCell Research Laboratories). The cells were seeded at 10000 cells/cm^2 on collagen-coated plates the day before 100 ng/mL testosterone treatment. Testosterone was dissolved in ethanol, and the final concentration of ethanol was adjusted to 0.1% (v/v) when used for cultured cells. The culture medium was replaced every 48 hours.

Cell proliferation curve

The seminal vesicle epithelial cells were seeded at 10000 cells/cm^2 and then were cultured in various concentrations of testosterone. The cells were washed with HBSS (without $CaCl_2$-$2H_2O$/$MgSO_4$) at the time of cell counting and collected using 0.25% (v/v) trypsin. The recovered cells were suspended in DMEM/F-12 medium, and cell numbers were determined using an Automated Cell Counter TC20TM (BIO-RAD Laboratories, Hercules, CA, USA) to calculate the number of cells contained per well (4 cm^2).

Cell cycle analysis

The recovered cells as described above were fixed in 2-5 ml of cold (4°C) 70% methanol for at least 30 minutes on ice. After centrifugation at 500g for 5 minutes at 4°C to obtain pellets, the cell pellet was suspended in 50 μM propidium iodide and 20 × diluted RNase (19101, QIAGEN Inc., Venlo, Netherlands) and then were incubated at 37°C for 30 minutes. After twice washing with 1 ml of PBS at 300 g for 3 min at 4°C, the cells were analyzed by flow cytometry. The cell population is shown in Supplementary Figure 9. A total of 20,000 events were analyzed.

RNA-sequencing

Total RNA was extracted from cells using the RNeasy Mini Kit (74106, QIAGEN) according to the manufacturer's protocol. Three independent samples were assayed to evaluate the reproducibility of the experimental procedures. The quality of total RNA (1 μg) submitted for sequencing was checked using a Bioanalyzer (Agilent Technologies Inc., Santa Clara, CA, USA), and all RNA integrity numbers were >7.0. The libraries for RNA sequencing were sequenced with 2 × 150-bp paired-end reads on a NovaSeq6000 (Illumina Inc., San Diego, CA, USA). The obtained sequencing data were analyzed using RaNA-seq *(58)*, an open bioinformatics tool for

rapid RNA-seq data analysis. FASTQ files were preprocessed in the pipeline using the Fastp tool, and expression was quantified using Salmon. DEseq2 was used to identify differentially expressed genes (DEGs) with adjusted p-values less than 0.05 between the testosterone-treated groups in transcripts per million (TPM) between control and testosterone-treated cells. The pathways were identified from the KEGG database on RaNA-seq.

Extracellular flux analysis

Oxygen consumption rate (OCR) and extracellular oxidation rate (ECAR) were measured using an extracellular flux analyzer (XF HS Mini; Agilent Technologies). Eight-well plates for the XF HS Mini were coated with fibronectin (5 µg/mL, F1141, Sigma-Aldrich) dissolved in phosphate-buffered saline (PBS), incubated overnight, and then washed with Roswell Park Memorial Laboratory medium for XF (Roswell Park Memorial Institute medium; RPMI, 103576-100, Agilent Technologies; containing 1% FBS) for XF before analysis. Mouse seminal vesicle epithelial cells or human seminal vesicle epithelial cells treated with 100 ng/mL testosterone for 7 days were suspended in RPMI medium at a concentration of 10,000 cells/180 µL, or mouse seminal vesicle epithelial cells infected with shRNA were suspended at a concentration of 2000 cells/180 µL in each well. After centrifugation at 300 × g for 3 minutes, the plates were placed in an incubator at 37°C and 100% air and used for analysis within 1 hour.

For glucose metabolism assessment, cells were sequentially treated as indicated with D-Glucose (10 mM; 103577-100, Agilent Technologies), Oligomycin (1 µM; O4876, Sigma-Aldrich), and 2-Deoxy-Glucose (50 mM; D8375, Sigma-Aldrich).

For mitochondrial respiration measurement, cells were sequentially treated as indicated with Oligomycin (1 µM), carbonyl cyanide 4-(trifluoromethoxy) phenylhydrazone (FCCP; 5 µM, SML2959, Sigma-Aldrich), and Rotenone (1 µM; R8875, Sigma-Aldrich)/Antimycin A (1 µM; A8674, Sigma-Aldrich). Cellular metabolism readouts, such as glycolysis, glycolytic capacity, glycolytic reserve, basal OCR, Maximum respiration, ATP Production, Spare respiratory capacity, were determined using the Agilent Seahorse Wave software.

For mouse sperm analysis, NaHCO3-free HTF medium was prepared according to Balbach et al. *(59)*. Plates were coated with concanavalin A (0.5 mg/mL, Fujifilm Wako Chemicals) overnight the day before assay. Each well was seeded with 180 µL of NaHCO3- Free HTF

medium containing 3,000,000 sperm cells. Sperm were injected with oleic acid (final concentration: 10 nM) with or without etomoxir (final concentration: 40 nM, E1905, Sigma-Aldrich).

Measurement of pyruvate and lactic acid

For measurements, mouse or human seminal vesicle epithelial cells were treated with 100 ng/ml testosterone for 6 days. The culture supernatant was collected after 24 hr of additional culture. Pyruvate consumption was measured using the Pyruvate Assay kit (MET-5029, Cell Biolabs, Inc., San Diego, CA, USA) according to the manufacturer's protocol. The fluorescence intensity was measured using a microplate reader (ex. 570 nm/em. 615 nm). Lactate released into the medium was measured using the Lactate Assay kit (L256, DOJINDO LABOLATORIES Co., Ltd., Kumamoto, Japan) according to the manufacturer's protocol. The absorbance was measured using a microplate reader (wave length=450nm).

qPCR

The cDNA was synthesized from 40 ng of total RNA using oligo$(dT)_{15}$ primers (3805, Takara Bio Inc., Shiga, Japan) and an Avian myeloblastosis virus (AMV) reverse transcriptase from Promega (M5101, Madison, WI, USA). The cDNA and primers were added to Power SYBR Green PCR Master Mix (4367659, Applied Biosystems, Foster City, CA, USA) in a total reaction volume of 15 μl. Conditions were set to the following parameters: 10 min at 95°C, 15 sec at 95°C, and 1 min at 60°C. Cycles were repeated 45 times. Specific primer pairs were selected and analyzed, as shown in Table S1. Expression was first normalized to housekeeping gene *Rpl19*, and fold change was calculated relative to the mean of the control samples.

Glucose uptake test of seminal vesicle epithelial cells and lipid determination of culture supernatants

Mouse or human seminal vesicle epithelial cells treated with or without 100 ng/mL testosterone for 6 days were used for this experiment. Cells were treated with or without the GLUT4 inhibitor indinavir (100 nM) and 100 ng/mL testosterone for an additional 24 hours. Collected 15,000 cells

were subjected to Glucose Uptake Assay Kit-Green (UP02; DOJINDO), and fluorescence intensity was measured using a microplate reader (ex. 485 nm/em. 535 nm).

Total lipid content in cultured medium was quantified using a lipid quantification kit (STA-617 Fluorometric, Cell Biolabs, Inc.) according to the manufacturer's protocol. The fluorescence intensity was measured using a microplate reader (ex. 485 nm/em. 535 nm).

Gas chromatography-mass spectrometry analysis

Fatty acid measurements in culture supernatant and seminal vesicle secretions were done according to our previous work *(18)*. Fatty acids in the samples were extracted and methylated using a fatty acid methylation kit (06482-04, Nacalai Tesque) and then purified using a fatty acid methyl ester purification kit (06483-94, Nacalai Tesque) according to the manufacturer's protocol. The methylated sample (3.0 mL) was dried and dissolved in 50 μL of elution solution. Samples were subjected to GC-MS.

Fatty acids were determined on an Agilent 7890A GC system coupled with a JMS-T 100 GCv mass detector at the Natural Science Research Center, Hiroshima University (N-BARD). Sample (1.0 μL aliquot) was injected to SP®-2560 capillary GC column (100 m × 0.25 mm i.d. × 0.2 μm film thickness; 24056, Sigma-Aldrich). For measurements, helium was used as the carrier gas at a constant flow rate of 2.0 mL/min. The GC oven temperature was gradually increased from 100°C to 300°C at a rate of 10°C/min and held at 300°C for 20 minutes. Ionization was performed using electron ionization with an electron energy of 70 eV. Mass spectra were obtained in scan mode (mass scan range 29-800 m/z). NIST MS Search v.2.0 was used to detect and identify of fatty acids.

Quantification of sperm oleic acid uptake by flow cytometry

To detect the fluorescence intensity of each sperm sample using flow cytometry, sperm collected from the epididymis were incubated with 1, 10 or 100 μM of fluorescently labeled oleic acid (F-OA-01, NANOCS, New York, NY, USA). After washing, fluorescence intensities were analyzed by flow cytometry using a 530/30 nm bandwidth filter and measured as mean intensity. A total of 100,000 sperm events were analyzed. The localization of fluorescence in sperm was determined using an APX100 Digital Imaging System.

ACLY knock down experiment using shRNA

The U6 shRNA lentiviral vector of the *Acly* gene (mAcly[shRNA#1]; a virus packaging service, VectorBuilder, Chicago, IL, USA) was used for knockdown experiments. The ACLY sequence targeted by the shRNA vector used in this study was 5′-GCAGCAAAGATGTTCAGTAAA-3′. Lentivirally transduced cells were prepared according to manufacture protocol. Immediately after isolation, the mouse seminal vesicle epithelial cells were cultured overnight in a medium containing 5 μg/mL polybrene (VectorBuilder) and lentiviral particles expressing an shRNA targeting ACLY or a scramble (Multiplicity of Infection of 10). After an additional overnight incubation in a fresh culture medium, the cells were incubated for 5 days in a medium containing 1 μg/ml puromycin (19752-64, Nacalai tesque). 100 ng/mL of testosterone was added to all procedures for the testosterone-treated group. Infection efficiency, calculated based on the number of GFP-positive cells using an APX100 Digital Imaging System, ranged between 70% and 90%.

Western blot analysis

Protein samples of mouse seminal vesicle epithelial cells and seminal vesicle tissue were prepared by homogenization in cell lysis buffer (04719964001, cOmplete™ Lysis-M EDTA-free, Roche) and diluted with an equal volume of sample buffer solution containing 2-ME (2 ×) for SDS-PAGE (30566-22, Nacalai tesque). The extracts (10 μg protein) were separated by SDS-polyacrylamide gel (10%) electrophoresis and transferred to polyvinylidene fluoride membranes (10600069, Cytiva, Tokyo, Japan). The membranes were then treated with Tris-buffered saline and Tween 20 (TBST, 20 mM Tris, pH 7.5, 150 mM NaCl, 0.1% Tween 20) containing 5% (w/v) Non-Fat Dry milk (MORINAGA MILK INDUSTRY Co., Ltd., Tokyo, Japan) for the nonspecific reaction was blocked. The membranes were incubated overnight at 4°C with primary antibodies: anti-ACLY antibody (1:10,000; ab40793; Abcam) or anti-α/β-Tubulin antibody (1:1,000; 2148S; Cell Signaling). The next day, membranes were washed with TBST and incubated with HRP-labeled antibody specific for rabbit IgG (1:4000; 7074S; Cell Signaling). The bands were visualized by using Enhanced Chemiluminescence detection systems

(RPN2232, Cytiva) and ChemiDoc™ MP Imaging System (BIO-RAD Laboratories). The bands were analyzed by using the software ImageJ (National Institutes of Health; Bethesda, MD, USA).

ATP production in sperm

After 1 hour of incubation in the presence or absence of oleic acid (10 nM), ATP in sperm was visualized by BioTracker ATP-Red (SCT045, Sigma-Aldrich). The sperm were incubated with 10 nM of working solution containing BioTracker ATP-Red dye at 37 °C for 60 min in the dark. After washing, the sperm pellet was resuspended in the base medium and analyzed with the flow cytometry using a 488 nm laser and a filter with a bandwidth of 574/26 nm. A total of 100,000 sperm events were analyzed. The sperm population is shown in Supplementary Figure 6.

Artificial insemination

To examine the involvement of seminal vesicle secretions in fertilization, sperm from C57BL/6N mice were injected directly into the uterine bodies of superovulated CD1 mice by syringe, as previously described with minor modifications *(14, 19)*. CD1 female mice were injected intraperitoneally with 8 IU eCG to stimulate follicle development and used as recipients for artificial insemination 48 hours later. Artificial seminal fluid was prepared in HTF medium to a final concentration of 10 mg/mL of collected control or frutamide-derived seminal vesicle secretions. As rescue experiment, 10 nM of oleic acid was added to the frutamide-derived seminal secretions. Cauda epididymis sperm was suspended with above artificial seminal fluid (1×10^6 sperm/mL), and a total of 40 µL (20 µL each per uterus) was injected through the cervix of the female mice. After artificial insemination, 7.5 IU of hCG was injected to stimulate ovulation. Subsequently, a mixture of vaseline and paraffin with a ratio of 10:1 was injected to form an artificial plug around the cervix. After 36~48 hours of sperm injection, the putative eggs were retrieved from the oviducts. The number of two-cell embryos and mature unfertilized eggs were counted and used to estimate the fertilization success rate.

Statistical analysis

Quantitative data were presented as means ± SEM. All statistical details of the experiments are given in the figure legends. R [(version 4.3.1 (2023-06-16)] was used for statistical analysis .

Data availability

Nucleotide sequence data reported are available in the DDBJ Sequenced Read Archive under the accession numbers DRA017090. Additional information needed to reanalyze the data reported in this paper is available from the principal contact upon request.

List of Supplementary Materials

Supplemental Figure 1 to 9

Table S1

Supplementary Data

Acknowledgments:

The authors would like to thank JoAnne S. Richards for carefully proofreading the manuscript and useful comments.

Funding:

This work was supported in part by JSPS KAKENHI Grant Number 23H00361 (to MS).

Author contributions:

Conceptualization: TY, TU, MS

Methodology: TY, ZX, NT, MA, TU

Investigation: TY, ZX, NT, MA, TU

Visualization: TY, MS

Funding acquisition: MS

Supervision: MS

Writing – original draft: TY

Writing – review & editing: TY, TU, MS

Competing interests:

MS holds stocks in and receives a salary from Hiroshima Cryopreservation Service Co. as a director. In addition, MS has received royalties and grants from Hiroshima Cryopreservation Service Co. M.S. has received consulting fees from Rohto Pharmaceutical Co., Ltd.. TU holds stocks in and receives a salary from Lullabio Inc. as a director and has received honoraria from Rohto Pharmaceutical Co., Ltd. The other authors declare they have no competing interests.

References

1. World Health Organization., Infertility prevalence estimates: 1990–2021. *Global report* , 1–98 (2023).

2. S. Elbashir, Y. Magdi, A. Rashed, R. Henkel, A. Agarwal, Epididymal contribution to male infertility: An overlooked problem. *Andrologia* **53**, e13721 (2021).

3. M. J. Cosentino, A. T. K. Cockett, Review Article: Structure and Function of the Epididymis Transport of Spermatozoa. *Urol Res* **14**, 229–240 (1986).

4. B. Howarth, Fertilizing ability of cock spermatozoa from the testis epididymis and vas deferens following intramagnal insemination. *Biol Reprod* **28**, 586–590 (1983).

5. S. Elbashir, Y. Magdi, A. Rashed, R. Henkel, A. Agarwal, Epididymal contribution to male infertility: An overlooked problem. *Andrologia* **53**, e13721 (2021).

6. T. G. Cooper, Sperm maturation in the epididymis: A new look at an old problem. *Asian J Androl* **9**, 533–539 (2007).

7. P. Gaddum-Rosse, Some observations on sperm transport through the uterotubal junction of the rat. *Am J Anat* **160**, 333–341 (1981).

8. R. Shalgi, T. T. Smith, R. Yanagimachi2, A Quantitative Comparison of the Passage of Capacitated and Uncapacitated Hamster Spermatozoa through the Uterotubal Junction. *Biol Reprod* **46**, 419–424 (1992).

9. H. Li, P. Hung, S. S. Suarez, Ejaculated Mouse Sperm Enter Cumulus-Oocyte Complexes More Efficiently In Vitro than Epididymal Sperm. (2015), doi:10.1371/journal.pone.0127753.

10. T. Noda, M. Ikawa, Physiological function of seminal vesicle secretions on male fecundity. *Reprod Med Biol* **18**, 241–246 (2019).

11. P. Verze, T. Cai, S. Lorenzetti, The role of the prostate in male fertility, health and disease. *Nat Rev Urol* **13**, 379–386 (2016).

12. E. Balandya, W. Wieland-Alter, K. Sanders, T. Lahey, Human Seminal Plasma Fosters CD4+ Regulatory T-cell Phenotype and Transforming Growth Factor-β1 Expression. *American Journal of Reproductive Immunology* **68**, 322–330 (2012).

13. T. Shima, K. Inada, A. Nakashima, A. Ushijima, M. Ito, O. Yoshino, S. Saito, Paternal antigen-specific proliferating regulatory T cells are increased in uterine-draining lymph nodes just before implantation and in pregnant uterus just after implantation by seminal plasma-priming in allogeneic mouse pregnancy. *J Reprod Immunol* **108**, 72–82 (2015).

14. N. Kawano, N. Araki, K. Yoshida, T. Hibino, N. Ohnami, M. Makino, S. Kanai, H. Hasuwa, M. Yoshida, K. Miyado, A. Umezawa, Seminal vesicle protein SVS2 is required for sperm survival in the uterus. *Proc Natl Acad Sci U S A* **111**, 4145–4150 (2014).

15. R. R. ROSECRANS, R. S. JEYENDRAN, M. PEREZ-PELAEZ, W. P. KENNEDY, Comparison of Biochemical Parameters of Human Blood Serum and Seminal Plasma. *Andrologia* **19**, 625–628 (1987).

16. T. Umehara, T. Kawai, M. Goto, J. A. S. Richards, M. Shimada, Creatine enhances the duration of sperm capacitation: a novel factor for improving in vitro fertilization with small numbers of sperm. *Human Reproduction* **33**, 1117–1129 (2018).

17. Z. Zhu, T. Kawai, T. Umehara, S. A. M. Hoque, W. Zeng, M. Shimada, Negative effects of ROS generated during linear sperm motility on gene expression and ATP generation in boar sperm mitochondria. *Free Radic Biol Med* **141**, 159–171 (2019).

18. M. M. Islam, T. Umehara, N. Tsujita, M. Shimada, Saturated fatty acids accelerate linear motility through mitochondrial ATP production in bull sperm. *Reprod Med Biol* **20**, 289–298 (2021).

19. T. Noda, Y. Fujihara, T. Matsumura, S. Oura, S. Kobayashi, M. Ikawa, Seminal vesicle secretory protein 7, PATE4, is not required for sperm function but for copulatory plug formation to ensure fecundity. *Biol Reprod* **100**, 1035–1045 (2019).

20. K. Queen, C. B. Dhabuwala, C. G. Pierrepoint, The effect of the removal of the various accessory sex glands on the fertility of male rats. *J Reprod Fertil* **62**, 423–426 (1981).

21. Mann T, Studies on the metabolism of semen; fructose as a normal constituent of seminal

plasma; site of formation and function of fructose in semen. *Biochem J* **40**, 481–491 (1946).

22. Humphrey GF, Mann T, Studies on the metabolism of semen; citric acid in semen. *Biochem J* **44**, 97–105 (1949).

23. C. Chang, S. O. Lee, R. S. Wang, S. Yeh, T. M. Chang, Androgen receptor (AR) physiological roles in male and female reproductive systems: lessons learned from AR-knockout mice lacking AR in selective cells. *Biol Reprod* **89**, 1–16 (2013).

24. C. Fix, C. Jordan, P. Cano, W. H. Walker, Testosterone activates mitogen-activated protein kinase and the cAMP response element binding protein transcription factor in Sertoli cells. *Proc Natl Acad Sci U S A* **101**, 10919–10924 (2004).

25. K. Nagaosa, A. Kishimoto, R. Kizu, A. Nakagawa, A. Shiratsuchi, Y. Nakanishi, Perturbation of spermatogenesis by androgen antagonists directly injected into seminiferous tubules of live mice. *Reproduction* **133**, 21–27 (2007).

26. L. B. Smith, W. H. Walker, The regulation of spermatogenesis by androgens. *Semin Cell Dev Biol* **30**, 2–13 (2014).

27. P. S. Cooke, W. H. Walker, Male fertility in mice requires classical and nonclassical androgen signaling. *Cell Rep* **36**, 109557 (2021).

28. S. P. Smyth, B. Nixon, A. L. Anderson, H. C. Murray, J. H. Martin, L. A. MacDougall, S. A. Robertson, D. A. Skerrett-Byrne, J. E. Schjenken, Elucidation of the protein composition of mouse seminal vesicle fluid. *Proteomics* **22**, e2100227 (2022).

29. H. Murata, P. W. Hruz, M. Mueckler, Indinavir inhibits the glucose transporter isoform Glut4 at physiologic concentrations. *AIDS* **16**, 859–863 (2002).

30. C. Wilson, A. Contreras-Ferrat, N. Venegas, C. Osorio-Fuentealba, M. Pávez, K. Montoya, J. Durán, R. Maass, S. Lavandero, M. Estrada, Testosterone increases GLUT4-dependent glucose uptake in cardiomyocytes. *J Cell Physiol* **228**, 2399–2407 (2013).

31. G. F. Gonzales, Function of seminal vesicles and their role on male fertility. *Asian J Androl* **3**, 251–258 (2001).

32. A. Lenzi, M. Picardo, L. Gandini, F. Dondero, Lipids of the sperm plasma membrane: from polyunsaturated fatty acids considered as markers of sperm function to possible scavenger therapy. *Hum Reprod Update* **2**, 246–256 (1996).

33. M. T. Haren, A. M. Siddiqui, H. J. Armbrecht, R. T. Kevorkian, M. J. Kim, M. J. Haas, A.

Mazza, V. B. Kumar, M. Green, W. A. Banks, J. E. Morley, Testosterone modulates gene expression pathways regulating nutrient accumulation, glucose metabolism and protein turnover in mouse skeletal muscle. *Int J Androl* **34**, 55–68 (2011).

34. L. C. Costello, R. B. Franklin, Testosterone and prolactin regulation of metabolic genes and citrate metabolism of prostate epithelial cells. *Horm Metab Res* **34**, 417–424 (2002).

35. K. Gonthier, R. T. K. Poluri, É. Audet-Walsh, Functional genomic studies reveal the androgen receptor as a master regulator of cellular energy metabolism in prostate cancer. *J Steroid Biochem Mol Biol* **191**, 105367 (2019).

36. M. F. Troncoso, M. Pavez, C. Wilson, D. Lagos, J. Duran, S. Ramos, G. Barrientos, P. Silva, P. Llanos, C. Basualto-Alarcón, B. D. Westenbrink, S. Lavandero, M. Estrada, Testosterone activates glucose metabolism through AMPK and androgen signaling in cardiomyocyte hypertrophy. *Biol Res* **54**, 1–16 (2021).

37. Chen X, Li X, Huang HY, Li X, Lin JF, Effects of testosterone on insulin receptor substrate-1 and glucose transporter 4 expression in cells sensitive to insulin. *Zhonghua Yi Xue Za Zhi* **86**, 1474–1477 (2006).

38. K. Sato, M. Iemitsu, K. Aizawa, R. Ajisaka, Testosterone and DHEA activate the glucose metabolism-related signaling pathway in skeletal muscle. *Am J Physiol Endocrinol Metab* **294**, E961–E968 (2008).

39. P. K. Arnold, B. T. Jackson, K. I. Paras, J. S. Brunner, M. L. Hart, O. J. Newsom, S. P. Alibeckoff, J. Endress, E. Drill, L. B. Sullivan, L. W. S. Finley, A non-canonical tricarboxylic acid cycle underlies cellular identity. *Nature* **603**, 477 (2022).

40. A. Luengo, Z. Li, D. Y. Gui, L. B. Sullivan, M. Zagorulya, B. T. Do, R. Ferreira, A. Naamati, A. Ali, C. A. Lewis, C. J. Thomas, S. Spranger, N. J. Matheson, M. G. Vander Heiden, Increased demand for NAD+ relative to ATP drives aerobic glycolysis. *Mol Cell* **81**, 691–707 (2021).

41. B. B. Yeap, Testosterone and cardiovascular disease risk. *Curr Opin Endocrinol Diabetes Obes* **22**, 193–202 (2015).

42. J. D. Marsh, M. H. Lehmann, R. H. Ritchie, J. K. Gwathmey, G. E. Green, R. J. Schiebinger, Androgen receptors mediate hypertrophy in cardiac myocytes. *Circulation* **98**, 256–261 (1998).

43. G. F. Grabner, H. Xie, M. Schweiger, R. Zechner, Lipolysis: cellular mechanisms for lipid mobilization from fat stores. *Nat Metab* **3**, 1445–1465 (2021).

44. B. Mittendorfer, Origins of metabolic complications in obesity: adipose tissue and free fatty acid trafficking. *Curr Opin Clin Nutr Metab Care* **14**, 535–541 (2011).

45. H. Wackerhage, I. J. Vechetti, P. Baumert, S. Gehlert, L. Becker, R. T. Jaspers, M. H. de Angelis, Does a Hypertrophying Muscle Fibre Reprogramme its Metabolism Similar to a Cancer Cell? *Sports Med* **52**, 2569–2578 (2022).

46. R. J. De Berardinis, N. S. Chandel, Fundamentals of cancer metabolism. *Sci Adv* **2**, e1600200 (2016).

47. G. L. Semenza, Hypoxia-inducible factors in physiology and medicine. *Cell* **148**, 399–408 (2012).

48. B. Morant-Ferrando, D. Jimenez-Blasco, P. Alonso-Batan, J. Agulla, R. Lapresa, D. Garcia-Rodriguez, S. Yunta-Sanchez, I. Lopez-Fabuel, E. Fernandez, P. Carmeliet, A. Almeida, M. Garcia-Macia, J. P. Bolaños, Fatty acid oxidation organizes mitochondrial supercomplexes to sustain astrocytic ROS and cognition. *Nature Metabolism 2023 5:8* **5**, 1290–1302 (2023).

49. M. Duta-Mare, V. Sachdev, C. Leopold, D. Kolb, N. Vujic, M. Korbelius, D. C. Hofer, W. Xia, K. Huber, M. Auer, B. Gottschalk, C. Magnes, W. F. Graier, A. Prokesch, B. Radovic, J. G. Bogner-Strauss, D. Kratky, Lysosomal acid lipase regulates fatty acid channeling in brown adipose tissue to maintain thermogenesis. *Biochim Biophys Acta Mol Cell Biol Lipids* **1863**, 467–478 (2018).

50. S. C. C. Huang, B. Everts, Y. Ivanova, D. O'Sullivan, M. Nascimento, A. M. Smith, W. Beatty, L. Love-Gregory, W. Y. Lam, C. M. O'Neill, C. Yan, H. Du, N. A. Abumrad, J. F. Urban, M. N. Artyomov, E. L. Pearce, E. J. Pearce, Cell-intrinsic lysosomal lipolysis is essential for alternative activation of macrophages. *Nat Immunol* **15**, 846–855 (2014).

51. K. H. Tsui, T. H. Feng, Y. F. Lin, P. L. Chang, H. H. Juang, p53 downregulates the gene expression of mitochondrial aconitase in human prostate carcinoma cells. *Prostate* **71**, 62–70 (2011).

52. S. Almeida, L. Rato, M. Sousa, M. G. Alves, P. F. Oliveira, Fertility and Sperm Quality in the Aging Male. *Curr Pharm Des* **23**, 4429–4437 (2017).

53. T. Murata, Y. Ishitsuka, K. Karouji, H. Kaneda, H. Toki, Y. Nakai, S. Makino, R. Fukumura, H. Kotaki, S. Wakana, T. Noda, Y. Gondo, β-cateninC429S mice exhibit sterility consequent to spatiotemporally sustained Wnt signalling in the internal genitalia. *Scientific Reports 2014 4:1* **4**,

1–7 (2014).

54. B. A. Stone, A. Alex, L. B. Werlin, R. P. Marrs, Age thresholds for changes in semen parameters in men. *Fertil Steril* **100**, 952–958 (2013).

55. J. L. Frattarelli, K. A. Miller, B. T. Miller, K. Elkind-Hirsch, R. T. Scott, Male age negatively impacts embryo development and reproductive outcome in donor oocyte assisted reproductive technology cycles. *Fertil Steril* **90**, 97–103 (2008).

56. A. P. Drabovich, P. Saraon, K. Jarvi, E. P. Diamandis, Seminal plasma as a diagnostic fluid for male reproductive system disorders. *Nat Rev Urol* **11**, 278–288 (2014).

57. T. Umehara, N. Tsujita, Z. Zhu, M. Ikedo, M. Shimada, A simple sperm-sexing method that activates TLR7/8 on X sperm for the efficient production of sexed mouse or cattle embryos. *Nat Protoc* **15**, 2645–2667 (2020).

58. C. Prieto, D. Barrios, RaNA-Seq: Interactive RNA-Seq analysis from FASTQ files to functional analysis. *Bioinformatics* **36**, 1955–1956 (2019).

59. M. Balbach, J. Buck, L. R. Levin, Using an Extracellular Flux Analyzer to Measure Changes in Glycolysis and Oxidative Phosphorylation during Mouse Sperm Capacitation. *J Vis Exp* **2020**, e60815 (2020).

Figures and Figure legends

Figure 1. Effects of seminal vesicle fluid and prostate fluids on sperm motility (A) To determine the effect of seminal plasma on sperm motility, we prepared "pseudo" seminal plasma from the mixture of seminal vesicle secretions or prostate extracts. (B-D) Tested various concentrations of these fluids on epididymal sperm: (B) Curvi-Linear Velocity; VCL, (C) Straight-Line Velocity; VSL and (D) Linearity; LIN is the ratio of VSL to VCL of sperm that was incubated with the mixture of seminal vesicle secretions and/or prostate extracts. (E) Experimental design to evaluate the effect of seminal secretions collected from male mice treated with or without flutamide (50 mg/kg subcutaneously for 7 days) on sperm. (F-H) Performed bioassay using seminal vesicle fluid after treatment with vehicle (Ctrl) or flutamide: (F) LIN, (G) VSL and (H) the activity of mitochondria were checked by JC-1 kit. Data are mean ± SEM. n=3-5 independent replicates. Significance was tested in comparison to HTF or Ctrl (vehicle-treated animals) using Student's t-test.

Figure 2. The testosterone-androgen receptor pathway inhibits the cell proliferation of seminal vesicle gland epithelial cells. (A) The localization of the androgen receptor (AR; NR3C4) in seminal vesicle of control (Ctrl) mice and those treated with flutamide (Fult). Scale bar=50 µm for left panel and 20 µm for right panel in each group. (B,C) Cell proliferation and apoptosis in seminal vesicle of control (Ctrl) mice and those treated with flutamide (Fult): (B) Representative images of Ctrl and Flut staining for Ki67 (top) and TUNEL (bottom). Scale bar=20 µm. (C) Percentage of Ki67 positive cells (top) and TUNEL positive (bottom) in Ctrl and Flut-treated seminal vesicle sections. (D) Experimental design to evaluate the effects of testosterone on the proliferation of seminal vesicle epithelial cells *in vitro*. The epithelial cells were culutured with or without testosterone for 8 days. (E) Growth curves of seminal vesicle epithelial cells that cultured with 0, 1, 10 and 100 ng/mL of testosterone. (F,G) Cell cycle status was determined by flow cytometry. Data are mean ± SEM. n=3-5 mice or independent replicates. Each replicate experiments with 3-6 wells containing pooled cells from 3-5 mice. Significance was tested in comparison to Ctrl using Student's t-test. The cell proliferation data were compared to Ctrl by Dunnett's test.

Figure 3. Testosterone changes the expression of genes involved in metabolic pathway in seminal vesicle epithelial cells. (A) Volcano plot of differentially expressed genes. RNA sequencing was performed using RNA extracted from the seminal vesicle epithelial cells cultured with or without 100 ng/mL testosterone. Genes with a significant expression change are highlighted as red dots. It found 4460 significant genes for a cutoff of $P<0.05$. (B) MA plot of differential expression results. The seminal vesicle specific genes are highlighted as red dots rather than significant genes. (C) Top 10 genes upregulated or downregulated by testosterone, respectively, for altered gene expression. (D) Conducted KEGG analysis to identify differences in pathway enrichment by testosterone, identifying the most variability in metabolic pathway genes. It shows the number of differential expressed genes annotated to Gene Ontology shows (x axis). p-value which measure the statistical significance of a possible functional enrichment for each term.

Figure 4. Testosterone regulates glucose metabolism and mitochondrial ATP production in seminal vesicle epithelial cells. (A-C) Glycolytic pathway analysis by an extracellular flux analyzer in seminal vesicle gland epithelial cells cultured with 100 ng/mL testosterone (Testo) or vehicle (Ctrl) for 7 days: (A) Extracellular acidification rate (ECAR) kinetics of seminal vesicle epithelial cells using an extracellular flux analyzer. (B) Glycolysis and (C) Glycolytic capacity. (D) Pyruvate concentration in the medium where seminal vesicle epithelial cells were cultured with or without testosterone for 24 hours. (E) Lactate concentration in the medium where seminal vesicle epithelial cells were cultured with or without testosterone for 24 hours. (F-J) Mitochondrial respiration measurement by an extracellular flux analyzer: (F) Oxygen consumption rate (OCR) kinetics of seminal vesicle epithelial cells with or without 100 ng/mL testosterone. (G) Basal OCR, (H) Maximum respiration, (I) Spare respiratory capacity and (J) ATP production. Data are mean ± SEM of $n = 3$ replicate experiments with 3-6 wells containing pooled cells from 3-5 mice or medium. Student's t-test was used to compare Ctrl and Testo.

Figure 5. Effect of testosterone on gene expression of enzymes involved in the glucose metabolic pathway in seminal vesicle epithelial cells. To elucidate the effects of testosterone on

gene expression of enzymes involved in glucose catabolism and anabolism in seminal vesicle gland epithelial cells. ctrl: 7 days of culture with vehicle. testo: 7 days of culture with 100 ng/mL testosterone. Data are mean ± SEM of n = 3 replicate experiments with 3-6 wells containing pooled cells from 3-5 mice. Student's t-test was used to compare Ctrl and Testo.

Figure 6. Oleic acid is incorporated to sperm, which enhances linear motility and mitochondrial activity. (A) Epididymal sperm were incubated with fluorescently labeled oleic acid (OA) and the fluorescence intensity after quenching was observed by a fluorescence microscope. (B) The fluorescence intensity of fluorescence-conjugated OA in sperm was detected by flow cytometry. (C) Average fluorescence intensity of sperm at different concentrations of fluorescence-conjugated OA. (D,E) OA improved sperm motility parameters. Sperm collected from mouse epididymis was incubated with OA for 60 min: (D) Straight-Line Velocity; VSL and (E) Linearity; LIN (F) Increase in the Oxygen consumption rate (OCR) after treatment with 10 nM OA or 10 nM OA + 40 nM Etomoxir (Eto). (G) The percentage of ATP-Red positive sperm after 1 hour incubation with or without 10 nM OA, measured using BioTracker ATP-Red staining and flow cytometry. (H) Artificial insemination using sperm treated with “pseudo” seminal plasma from control (SV), flutamide-treated (Flu) mice and supplement of OA (Flu+OA) followed by an evaluation of the fertilization rates. Data are mean ± SEM. n=3-6 independent replicates. Student's t-test was used for comparison between the two groups.

Figure 7. Testosterone-regulated ACLY induces metabolic shifts in seminal vesicle epithelial cells. (A) Western blot images of ACLY and α/β-tubulin in three sets of seminal vesicle epithelial cells cultured with 100 ng/mL testosterone (Testo) or in vehicle (Ctrl) for 7 days. (B) Quantitative analysis of ACLY relative to α-tubulin obtained from Western blot. (C) siRNA knockdown experiments of ACLY in seminal vesicle epithelial cells. ACLY protein levels in scrambled shRNA or ACLY shRNA-transfected seminal vesicle epithelial cells cultured with or without 100 ng/mL testosterone were determined by Western blot. (D-F) Changes in oxygen consumption of seminal epithelial cells were analyzed by a flux analyzer: (D) Oxygen consumption rate (OCR) kinetics of seminal vesicle epithelial cells transfected with scrambled shRNA or ACLY shRNA. (E) Basal OCR and (F) Maximum respiration. (G) The impact of ACLY knockdown on

testosterone-induced fatty acid synthesis was measured. (H) The effect of culture supernatants of testosterone-treated cells on sperm motility was evaluated, especially after ACLY knockdown. Curvi-Linear Velocity; VCL, Straight-Line Velocity; VSL, Linearity; LIN. Data are mean ± SEM. n=3-6 independent replicates. Repeated experiments were performed with cells recovered from 3 wells containing pooled cells from 3 to 5 mice. Student's t-test was used for comparison between the two groups.

Figure 8. Testosterone regulates the metabolic activity of human seminal epithelial cells. (A) Representative image of human seminal vesicle epithelial cells. (B) Growth curves of seminal vesicle epithelial cells with 100 ng/mL testosterone. (C) Oxygen consumption rate (OCR) kinetics and (D) Extracellular acidification rate (ECAR) kinetics of human seminal vesicle epithelial cells after 6 days of culture with or without 100 ng/mL testosterone using a flux analyzer. (E) Effects of testosterone on fluorescent glucose uptake and inhibitors of GLUT4 function. (F) Effects of testosterone and GLUT4 inhibitors on fatty acid synthesis. Data are mean ± SEM. n=3 independent replicates. Student's t-test was used for comparison between the two groups.

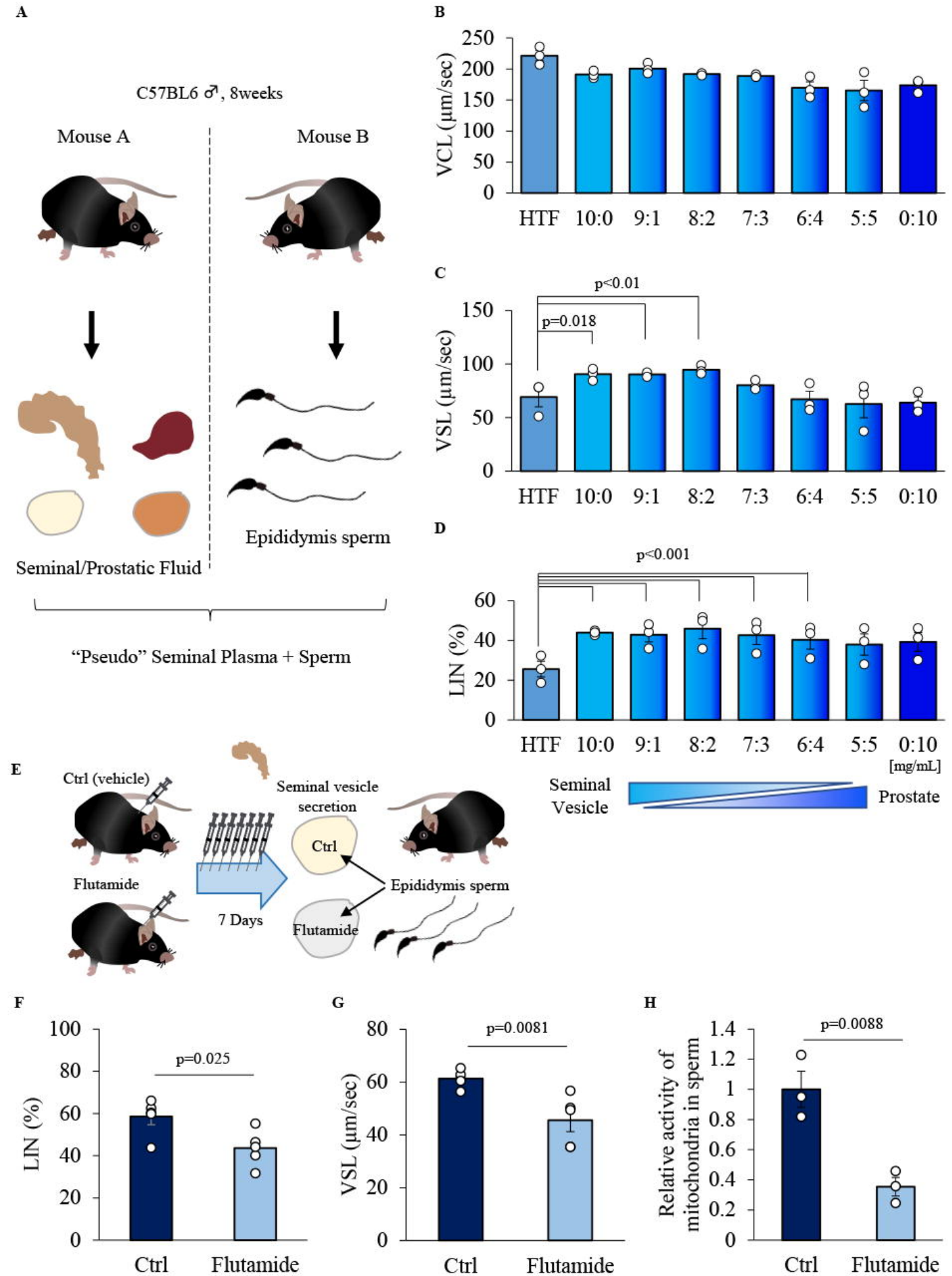
A
C57BL6 ♂, 8weeks
Mouse A
Mouse B
Epididymis sperm
Seminal/Prostatic Fluid
"Pseudo" Seminal Plasma + Sperm
B
VCL (µm/sec)
250
200
150
100
50
0
HTF
10:0
9:1
8:2
7:3
6:4
5:5
0:10
C
p<0.01
p=0.018
VSL (µm/sec)
150
100
50
0
HTF
10:0
9:1
8:2
7:3
6:4
5:5
0:10
D
p<0.001
LIN (%)
60
40
20
0
HTF
10:0
9:1
8:2
7:3
6:4
5:5
0:10
[mg/mL]
Seminal Vesicle
Prostate
E
Ctrl (vehicle)
Flutamide
7 Days
Seminal vesicle secretion
Ctrl
Flutamide
Epididymis sperm
F
LIN (%)
100
80
60
40
20
0
p=0.025
Ctrl
Flutamide
G
VSL (µm/sec)
80
60
40
20
0
p=0.0081
Ctrl
Flutamide
H
Relative activity of mitochondria in sperm
1.4
1.2
1
0.8
0.6
0.4
0.2
0
p=0.0088
Ctrl
Flutamide

Figure 1

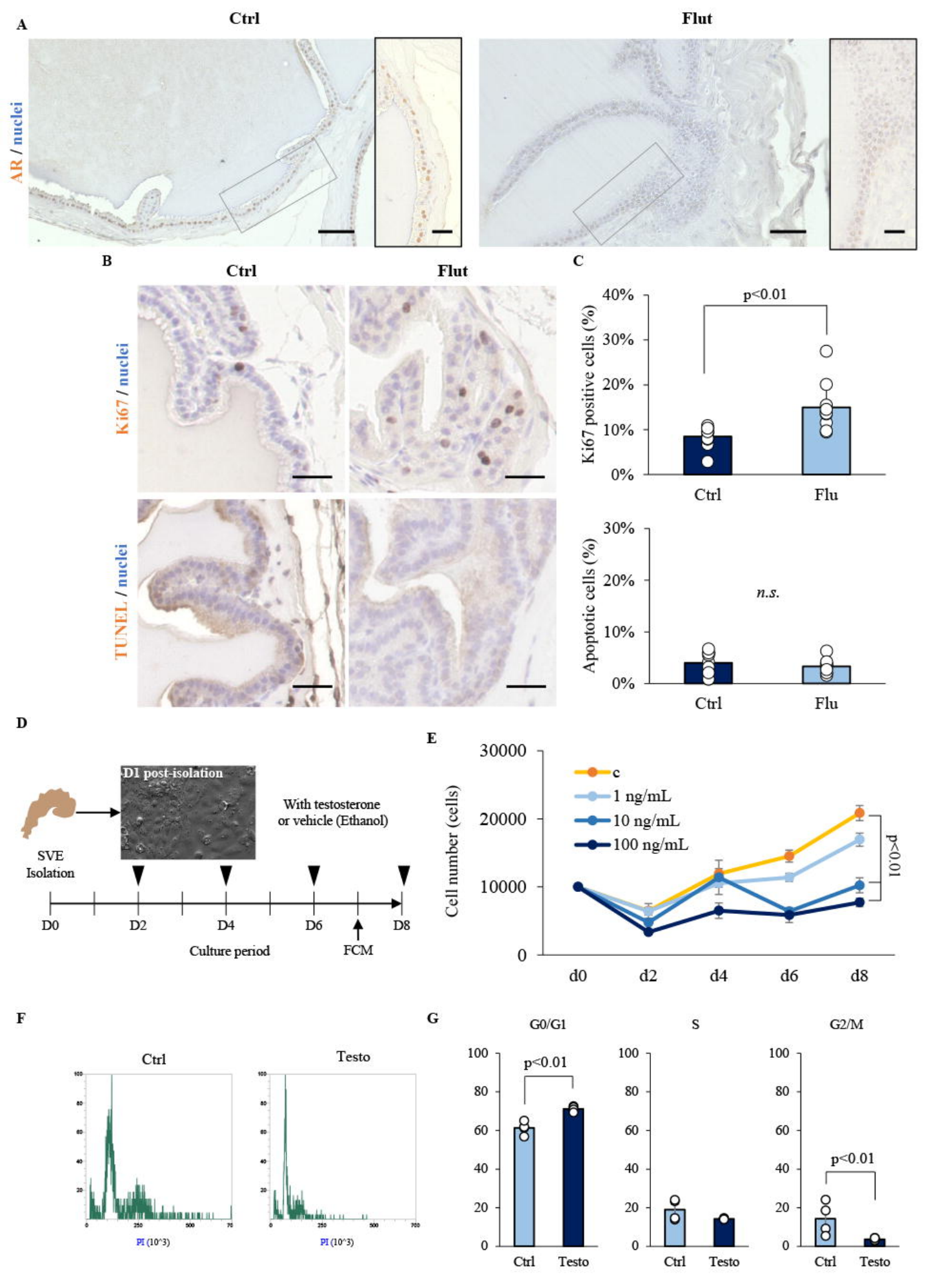
A
Ctrl
Flut
AR / nuclei
B
Ctrl
Flut
Ki67 / nuclei
TUNEL / nuclei
C
p<0.01
Ki67 positive cells (%)
40%
30%
20%
10%
0%
Ctrl
Flu
Apoptotic cells (%)
30%
20%
10%
0%
n.s.
Ctrl
Flu
D
D1 post-isolation
With testosterone
or vehicle (Ethanol)
SVE
Isolation
D0
D2
D4
D6
D8
Culture period
FCM
E
Cell number (cells)
30000
20000
10000
0
c
1 ng/mL
10 ng/mL
100 ng/mL
p<0.01
d0
d2
d4
d6
d8
F
Ctrl
Testo
PI (10^3)
PI (10^3)
G
G0/G1
S
G2/M
p<0.01
p<0.01
Ctrl
Testo
Ctrl
Testo
Ctrl
Testo

Figure 2

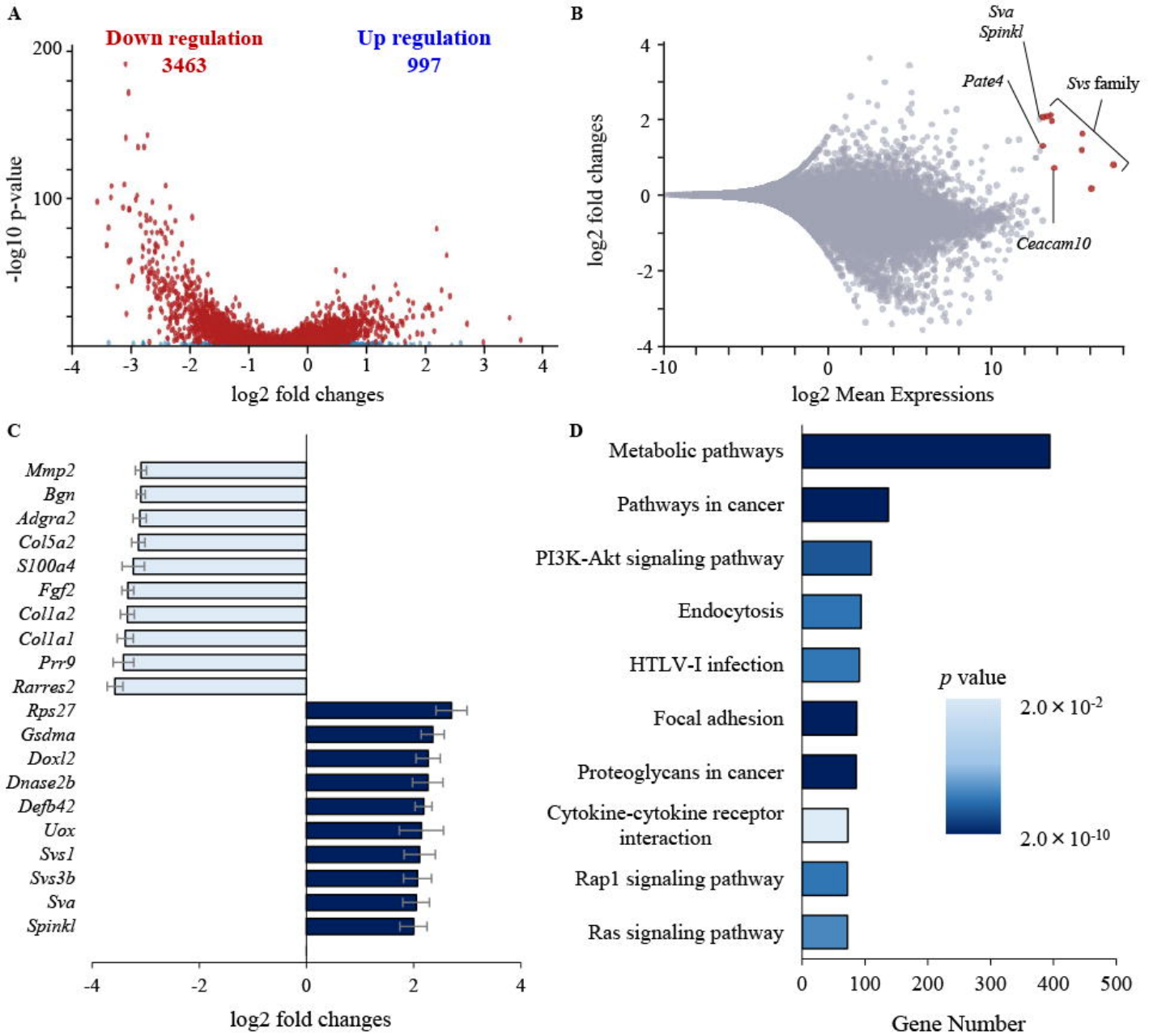
A
Down regulation
3463
Up regulation
997
-log10 p-value
log2 fold changes
B
Sva
Spinkl
Pate4
Svs family
Ceacam10
log2 fold changes
log2 Mean Expressions
C
Mmp2
Bgn
Adgra2
Col5a2
S100a4
Fgf2
Col1a2
Col1a1
Prr9
Rarres2
Rps27
Gsdma
Doxl2
Dnase2b
Defb42
Uox
Svs1
Svs3b
Sva
Spinkl
log2 fold changes
D
Metabolic pathways
Pathways in cancer
PI3K-Akt signaling pathway
Endocytosis
HTLV-I infection
Focal adhesion
Proteoglycans in cancer
Cytokine-cytokine receptor interaction
Rap1 signaling pathway
Ras signaling pathway
p value
2.0 × 10-2
2.0 × 10-10
Gene Number

Figure 3

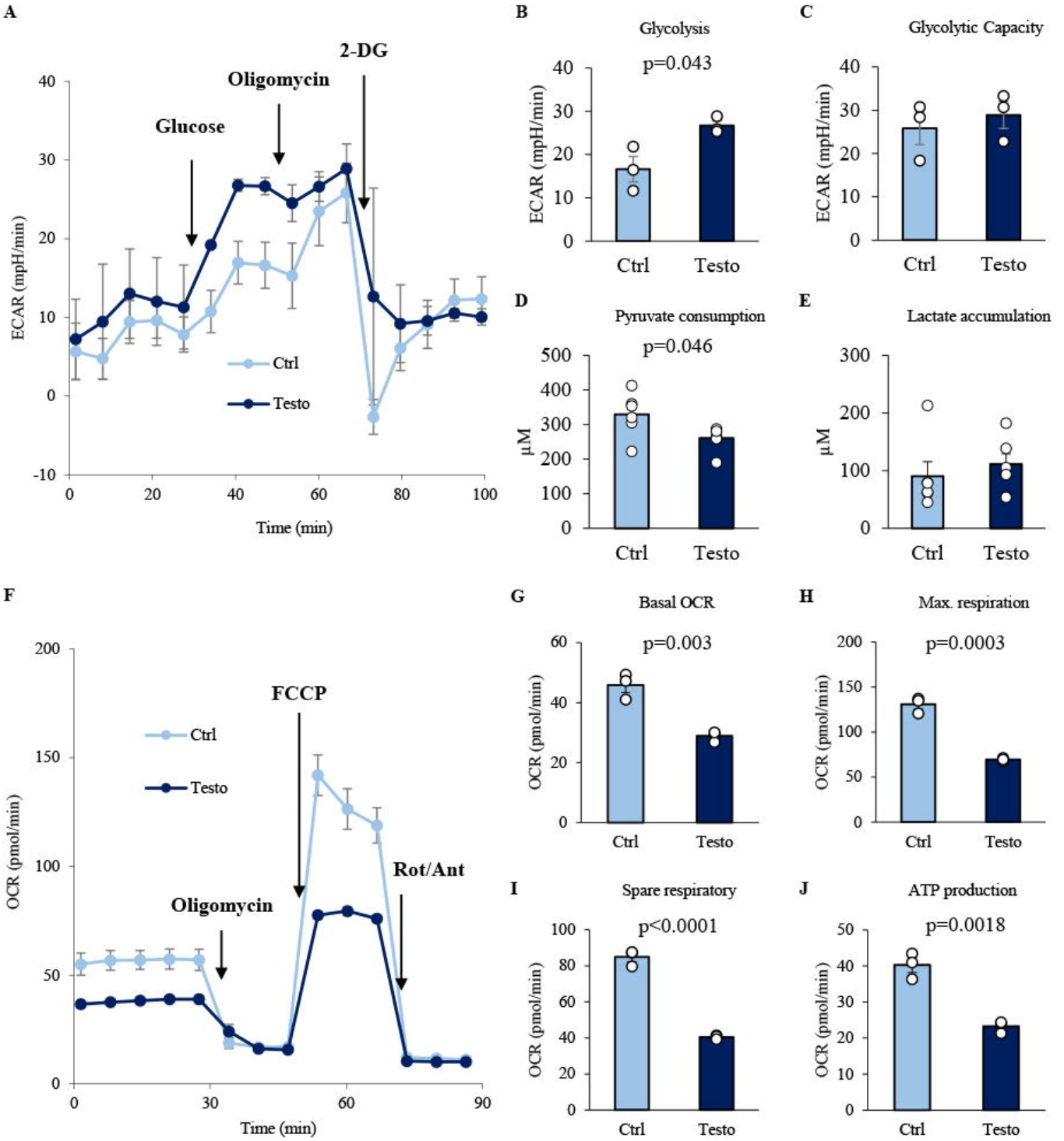
A
Glucose
Oligomycin
2-DG
ECAR (mpH/min)
Time (min)
Ctrl
Testo
B
Glycolysis
p=0.043
ECAR (mpH/min)
Ctrl
Testo
C
Glycolytic Capacity
ECAR (mpH/min)
Ctrl
Testo
D
Pyruvate consumption
p=0.046
µM
Ctrl
Testo
E
Lactate accumulation
µM
Ctrl
Testo
F
FCCP
Oligomycin
Rot/Ant
Ctrl
Testo
OCR (pmol/min)
Time (min)
G
Basal OCR
p=0.003
OCR (pmol/min)
Ctrl
Testo
H
Max. respiration
p=0.0003
OCR (pmol/min)
Ctrl
Testo
I
Spare respiratory
p<0.0001
OCR (pmol/min)
Ctrl
Testo
J
ATP production
p=0.0018
OCR (pmol/min)
Ctrl
Testo

Figure 4

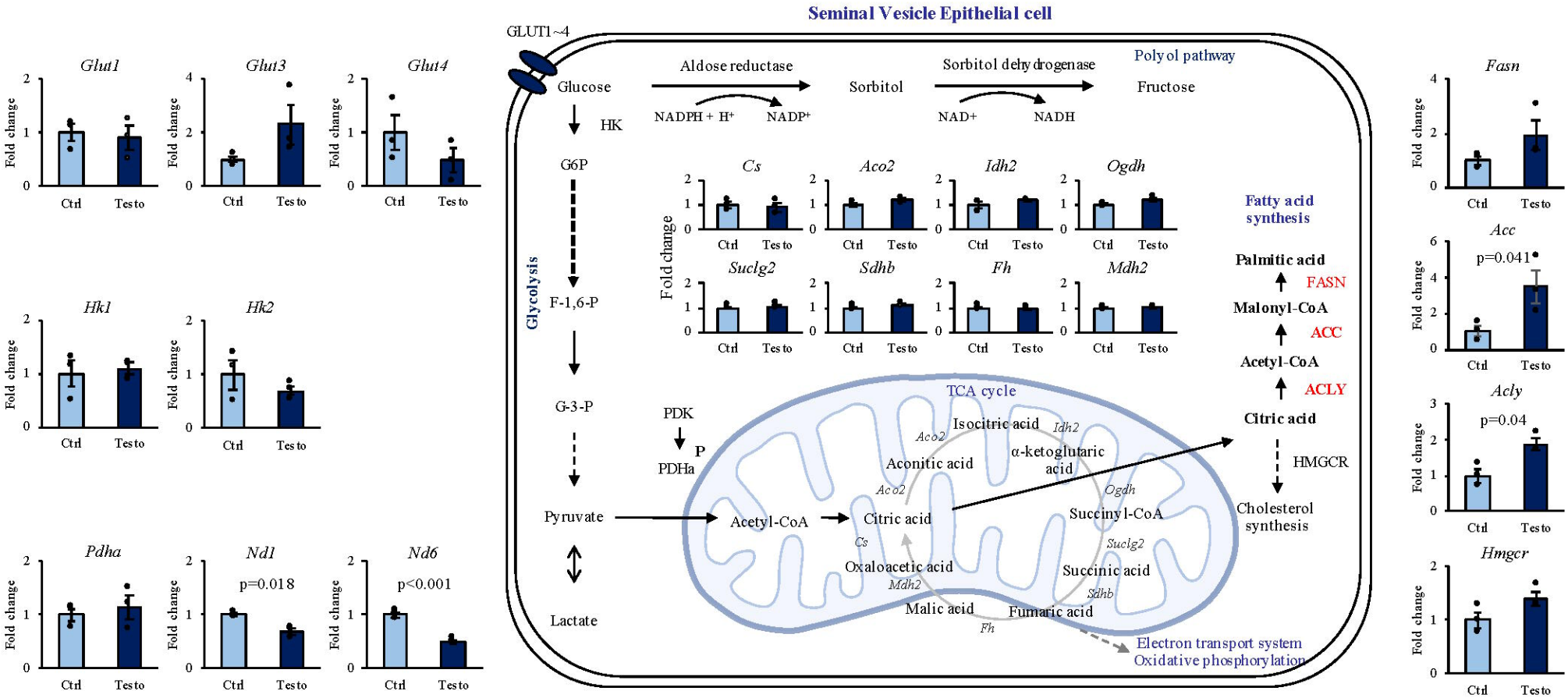
Glut1
Glut3
Glut4
Hk1
Hk2
Pdha
Nd1
p=0.018
Nd6
p<0.001
Fold change
Ctrl
Testo
Seminal Vesicle Epithelial cell
GLUT1~4
Glucose
HK
G6P
F-1,6-P
G-3-P
Pyruvate
Lactate
Glycolysis
Aldose reductase
NADPH + H+
NADP+
Sorbitol
Sorbitol dehydrogenase
NAD+
NADH
Fructose
Polyol pathway
Cs
Aco2
Idh2
Ogdh
Suclg2
Sdhb
Fh
Mdh2
PDK
PDHa
P
Acetyl-CoA
TCA cycle
Isocitric acid
Aconitic acid
α-ketoglutaric acid
Citric acid
Succinyl-CoA
Oxaloacetic acid
Succinic acid
Malic acid
Fumaric acid
Electron transport system
Oxidative phosphorylation
Fatty acid synthesis
Palmitic acid
FASN
Malonyl-CoA
ACC
Acetyl-CoA
ACLY
Citric acid
HMGCR
Cholesterol synthesis
Fasn
Acc
p=0.041
Acly
p=0.04
Hmgcr

Figure 5

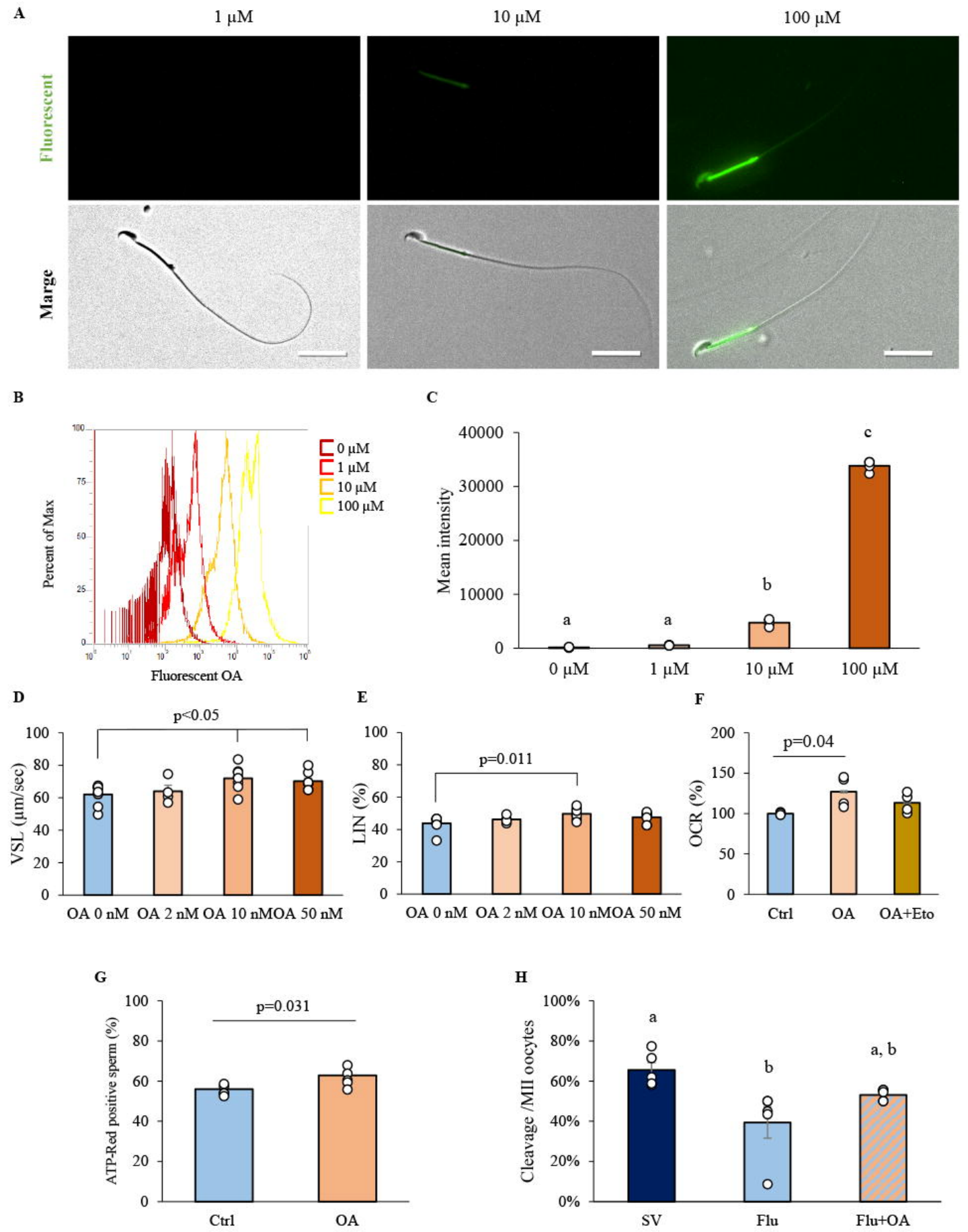
A
1 µM
10 µM
100 µM
Fluorescent
Marge
B
Percent of Max
Fluorescent OA
0 µM
1 µM
10 µM
100 µM
C
Mean intensity
a
a
b
c
0 µM
1 µM
10 µM
100 µM
D
p<0.05
VSL (µm/sec)
OA 0 nM
OA 2 nM
OA 10 nM
OA 50 nM
E
p=0.011
LIN (%)
OA 0 nM
OA 2 nM
OA 10 nM
OA 50 nM
F
p=0.04
OCR (%)
Ctrl
OA
OA+Eto
G
p=0.031
ATP-Red positive sperm (%)
Ctrl
OA
H
Cleavage /MII oocytes
a
b
a, b
SV
Flu
Flu+OA

Figure 6

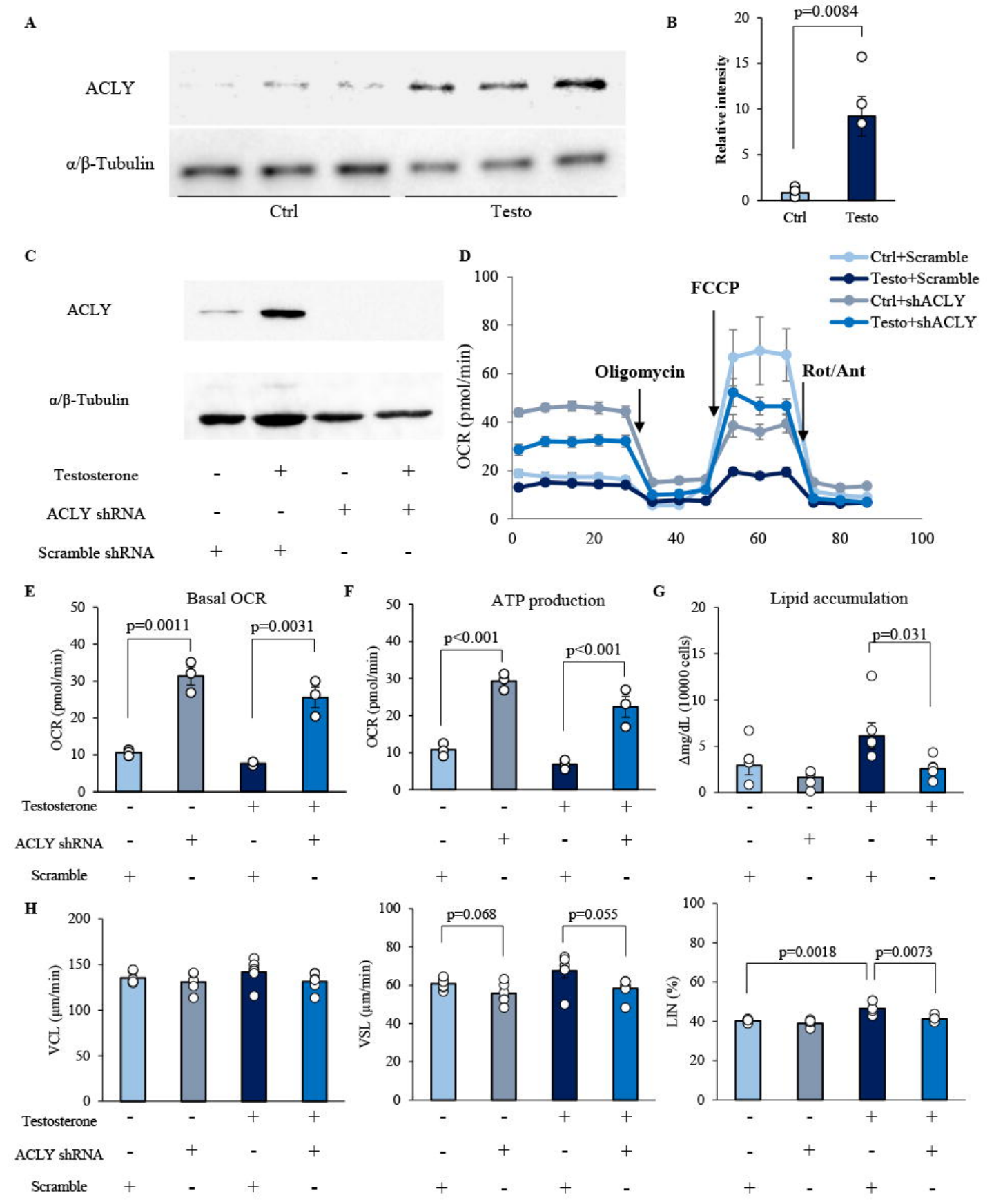
A
ACLY
α/β-Tubulin
Ctrl
Testo
B
p=0.0084
Relative intensity
Ctrl
Testo
C
ACLY
α/β-Tubulin
Testosterone
ACLY shRNA
Scramble shRNA
D
Ctrl+Scramble
Testo+Scramble
Ctrl+shACLY
Testo+shACLY
FCCP
Oligomycin
Rot/Ant
OCR (pmol/min)
E
Basal OCR
p=0.0011
p=0.0031
OCR (pmol/min)
F
ATP production
p<0.001
p<0.001
OCR (pmol/min)
G
Lipid accumulation
p=0.031
Δmg/dL (10000 cells)
H
VCL (μm/min)
p=0.068
p=0.055
VSL (μm/min)
p=0.0018
p=0.0073
LIN (%)

Figure 7

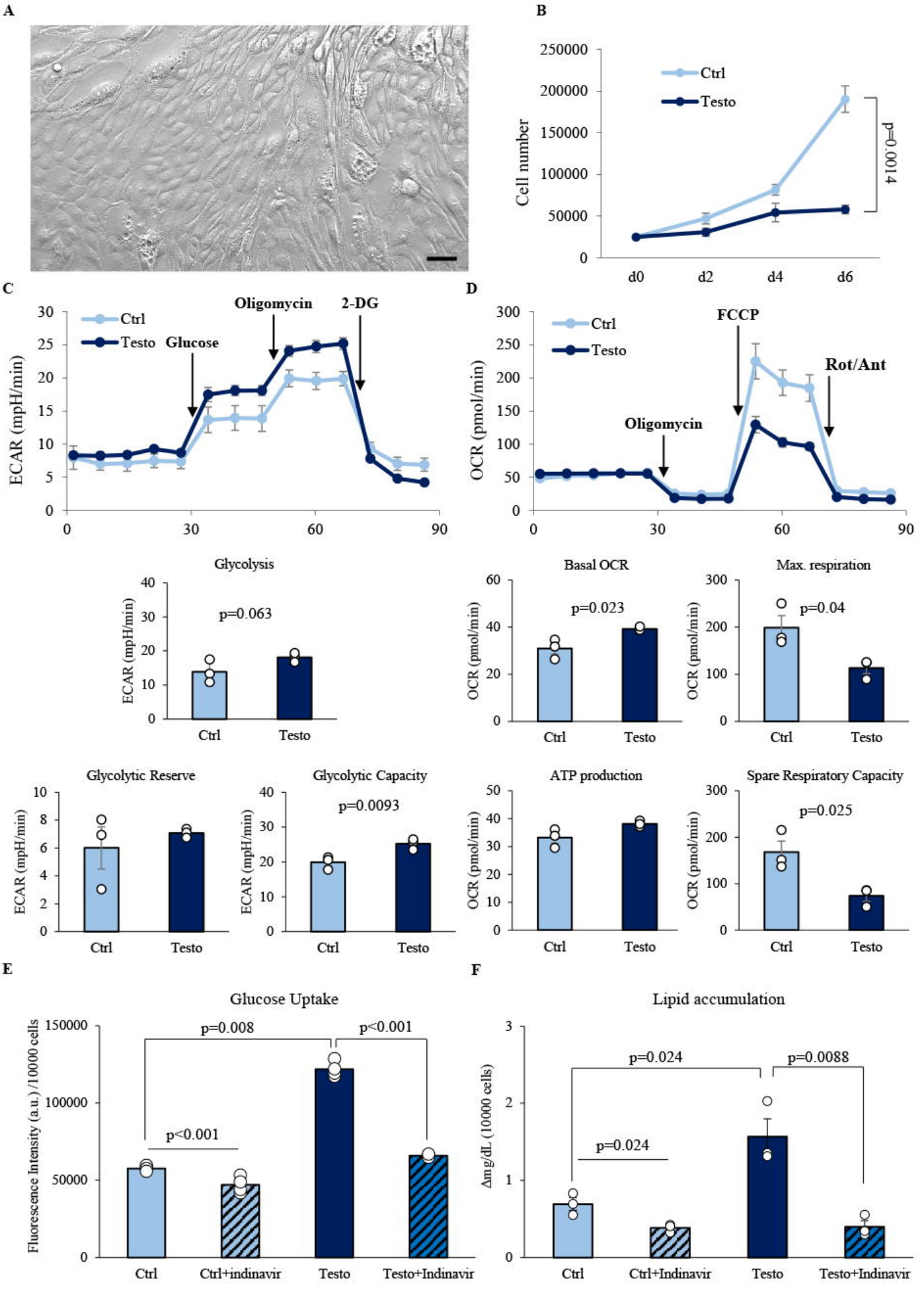
A
B
Ctrl
Testo
Cell number
250000
200000
150000
100000
50000
0
d0
d2
d4
d6
p=0.0014
C
Ctrl
Testo
Glucose
Oligomycin
2-DG
ECAR (mpH/min)
D
Ctrl
Testo
FCCP
Rot/Ant
Oligomycin
OCR (pmol/min)
Glycolysis
p=0.063
ECAR (mpH/min)
Basal OCR
p=0.023
OCR (pmol/min)
Max. respiration
p=0.04
OCR (pmol/min)
Glycolytic Reserve
ECAR (mpH/min)
Glycolytic Capacity
p=0.0093
ECAR (mpH/min)
ATP production
OCR (pmol/min)
Spare Respiratory Capacity
p=0.025
OCR (pmol/min)
Ctrl
Testo
E
Glucose Uptake
Fluorescence Intensity (a.u.)/10000 cells
p=0.008
p<0.001
p<0.001
Ctrl
Ctrl+indinavir
Testo
Testo+Indinavir
F
Lipid accumulation
Δmg/dL (10000 cells)
p=0.024
p=0.0088
p=0.024
Ctrl
Ctrl+Indinavir
Testo
Testo+Indinavir

Figure 8